Design of a dynamic positioning system for a floating body

Design of a Dynamic Positioning System for a Floating Body

R.M.C. Mestrom

Report no. DCT. 2004.10

Research report

Coaches: Prof. Dr.-Ing. E. Kreuzer[†]
Prof.dr. H. Nijmeijer[‡]
Dipl.-Ing. M.-A. Pick[†]

[†]Technical University Hamburg-Harburg
Department of Mechanics and Ocean Engineering

[‡]Eindhoven University of Technology
Department of Mechanical Engineering
Dynamics and Control Group

Eindhoven, January 2004

Contents

Abstract

In marine applications, it is often necessary that a vessel maintains its position and orientation in the sea or follows a certain reference trajectory. Examples of such vessels are cable-layers, ice-breakers and offshore supply vessels. Moreover, nowadays freely floating oil drilling platforms are built, which can operate in seas where the water depth is too large for maintaining position merely by means of anchors. This positioning and orientation keeping issue demands for a so-called dynamic positioning (DP) system which maintains the desired position exclusively by means of active thrusters.

In this project, the subject of the dynamic positioning system is a floating body, which will be used to investigate the rolling behaviour of ships. A model of this body is derived, describing the motion of the floating body with three degrees of freedom. Furthermore, the influence of the environmental disturbances (waves) on the body is included. These disturbances consist of two important contributions, namely an oscillatory wave motion and wave drift. As the dynamic positioning system only has to compensate for the drift, certain filtering properties have to be included, which are achieved by using both a controller and an observer.

Using Lyapunov methods, the controller and observer are designed and the dynamic positioning system is proven to be stable in a global sense for bounded yaw-rates. Simulations with the complete system confirm this.

The DP system is implemented on an experimental setup, in which thrusters are used as actuators. Identification of these thrusters reveals threshold values in the characteristics. Due to this, and some other hardware problems, the lateral and rotational degree of freedom cannot be controlled at the same time. The experiments, in which only the two translational degrees of freedom are controlled, show that the body can be stabilised to within a small region around the origin, thus achieving a satisfactory control result.

Samenvatting

In marinetoepassingen is het vaak nodig dat een vaartuig zijn positie en oriëntatie in zee vasthoudt of een bepaalde trajectorie volgt. Voorbeelden van zulke vaartuigen zijn kabel-leggers, ijsbrekers en bevoorradingsschepen. Bovendien worden er tegenwoordig vrij drijvende olieplatformen gebouwd, die in zeeën kunnen opereren waar de waterdiepte te hoog is om alleen door middel van ankers de positie vast te houden. Dit probleem van positioneren en oriëntatie houden, vraagt om een zogenaamd dynamisch positioneer (DP) systeem, waarbij de gewenste positie exclusief wordt vastgehouden door middel van actieve thrusters.

In dit project is het onderwerp van het dynamisch positioneer systeem een drijvend lichaam, hetgeen gebruikt zal worden voor het onderzoeken van rol-gedrag van schepen. Er is een model van dit lichaam afgeleid, dat de bewegingen van het drijvend lichaam met drie vrijheidsgraden beschrijft. Bovendien is de invloed van verstoringen ten gevolge van de omgeving (golven) toegevoegd. Deze verstoringen bestaan uit twee belangrijke bijdragen, namelijk een oscillerende golfbeweging en drift. Aangezien het dynamisch positioneer systeem alleen maar hoeft te compenseren voor de drift, moeten bepaalde filterende eigenschappen toegevoegd worden, welke bereikt worden door het gebruik van zowel een regelaar als een waarnemer.

De regelaar en waarnemer zijn ontworpen gebruik makend van Lyapunov methoden en stabiliteit van het dynamisch positioneer systeem is in globale zin aangetoond voor begrensde giersnelheden. Simulaties met het complete systeem bevestigen dit.

Het DP systeem is getest op een experimentele opstelling, waarin thrusters worden gebruikt als actuatoren. Identificatie van deze thrusters duidt op drempelwaarden in hun karakteristieken. Hierdoor, en door enkele andere hardware problemen, kunnen de laterale en rotationele vrijheidsgraad niet tegelijkertijd geregeld worden. De experimenten, waarin slechts de twee translerende vrijheidsgraden geregeld worden laten zien dat het lichaam gestabiliseerd kan worden tot in een klein gebied rond de oorsprong, waarmee een voldoende regelresultaat bereikt wordt.

Notation

General Notation

a, A	scalar
$\boldsymbol{a}$	(column) vector
$\boldsymbol{A}$	matrix
$\mathbf{0}$	null vector or matrix
$\boldsymbol{I}$	unit matrix
$\boldsymbol{a}^T$, $\boldsymbol{A}^T$	transpose of a vector $\boldsymbol{a}$ or matrix $\boldsymbol{A}$
$\boldsymbol{A}^{-1}$	inverse of a matrix $\boldsymbol{A}$
$\dot{a}$	total derivative of a with respect to time t
$\hat{a}$	estimate of a
$\tilde{a}$	$= a - \hat{a}$, estimation error in parameter a
$f(\cdot)$	scalar function of one variable
$\lambda_{max}(\boldsymbol{A})$, $\lambda_{min}(\boldsymbol{A})$	largest, smallest eigenvalue of $\boldsymbol{A}$, respectively
$\lvert a \rvert$	absolute value of a
$\lVert \cdot \rVert$	Euclidian norm (for matrices, $\lVert \boldsymbol{A} \rVert = \sqrt{\lambda_{max}(\boldsymbol{A}^T\boldsymbol{A})}$ is used)
$\mathbb{R}$	collection of real numbers

Latin Symbols

a_{ji}	$i = 1, 2, 3$, $j = 1, \ldots, 5$; transfer function coefficients
$\boldsymbol{b}$	vector with bias forces and moments
f_i	thruster forces
f_{0i}, f_{1i}	thruster curve parameters
$\boldsymbol{g}(\boldsymbol{\eta})$	vector with restoring forces and moments
$\boldsymbol{g}(\boldsymbol{q}, \tilde{\boldsymbol{q}})$	vectorial function with perturbation terms
$\boldsymbol{g}_1$, $\boldsymbol{g}_2$	vectors with perturbation terms
$h(s)$	wave transfer function approximation

k_{ji}	$i = 1, 2, 3$, $j = 1, \ldots, 7$; elements of the observer gain matrices
l_i	$i = 1, \ldots, 6$; wire length
m	system mass
n	input value
p	angular velocity about x-axis
q	angular velocity about y-axis
$\boldsymbol{q}$	vectorial concatenation of $\boldsymbol{\xi}$, $\boldsymbol{\eta}_e$ and $\boldsymbol{\nu}_e$
r	angular velocity about z-axis
r_{max}	maximum allowable yaw rate
t	time
u	velocity in x-direction
$\boldsymbol{u}$	input vector
v	velocity in y-direction
$\boldsymbol{v}$	vector with zero-mean Gaussian white measurement noise
w	velocity in z-direction
$\boldsymbol{w}$	vector with zero-mean Gaussian white noise
x	x-position
x_G	body-fixed distance from the origin to the centre of gravity
$\boldsymbol{x}_0$	vectorial concatenation of $\boldsymbol{x}_w$ and $\boldsymbol{\eta}$
$\boldsymbol{x}$	vectorial concatenation of $\boldsymbol{x}_0$ and $\boldsymbol{b}$
y	y-position
$\boldsymbol{y}$	output
z	z-position
$\boldsymbol{z}$	linear combination of $\boldsymbol{y}$ and $\boldsymbol{b}$
	linear transformation ($\boldsymbol{z} = \boldsymbol{T}(\psi)\boldsymbol{x}$)
$\boldsymbol{A}$	system matrix
$\boldsymbol{B}$	input matrix
$\boldsymbol{B}_\tau$	thruster configuration matrix
$\boldsymbol{C}$	output matrix
$\boldsymbol{C}(\boldsymbol{\nu})$	matrix with Coriolis and centripetal terms
$\boldsymbol{D}(\boldsymbol{\nu})$, $\boldsymbol{D}$	damping matrix
$\boldsymbol{D}(\boldsymbol{\nu})_P$	potential damping
$\boldsymbol{D}(\boldsymbol{\nu})_S$	damping due to skin friction
$\boldsymbol{D}(\boldsymbol{\nu})_V$	damping due to vortex shedding
$\boldsymbol{D}(\boldsymbol{\nu})_W$	damping due to wave drift
$\boldsymbol{E}$	intensity scaling matrix

$\boldsymbol{H}(s)$	transfer function matrix
$\boldsymbol{J}(\boldsymbol{\eta})$, $\boldsymbol{J}_1(\boldsymbol{\eta}_1)$, $\boldsymbol{J}_2(\boldsymbol{\eta}_2)$	rotation matrices
K	moment about x-axis
$\boldsymbol{K}_p$	proportional gain matrix
$\boldsymbol{K}_i$	integral gain matrix
	$i = 1, 2, 3, 4$; observer gain matrices
$\boldsymbol{K}_d$	derivative gain matrix
M	moment about y-axis
$\boldsymbol{M}$	mass matrix
N	moment about z-axis
	added inertia coefficient in r-direction
O	origin
$\boldsymbol{P}$	positive definite matrix
$\boldsymbol{Q}$	positive definite matrix
$\boldsymbol{S}$, $\boldsymbol{S}_T$	skew-symmetric matrix used for $\dot{\boldsymbol{J}}(\psi)$ and $\dot{\boldsymbol{T}}(\psi)$, respectively
$\boldsymbol{T}$	diagonal matrix with time constants
$\boldsymbol{T}(\psi)$	rotation matrix
V	(candidate) Lyapunov function
X	force in x-direction
	added mass coefficient in x-direction
XYZ	earth-fixed reference frame
$X_0Y_0Z_0$	body-fixed reference frame
Y	force in y-direction
	added mass coefficient in y-direction
Z	force in z-direction

Greek Symbols

γ	scalar tuning parameter
$\boldsymbol{\varepsilon}_{\tilde{z}}$, $\boldsymbol{\varepsilon}_{\tilde{\nu}}$	error vectors depending on $\tilde{\boldsymbol{z}}$ and $\tilde{\boldsymbol{\nu}}$, respectively
$\boldsymbol{\eta}$	position and orientation vector
θ	rotation around y-axis
$\theta_1(\cdot)$, $\theta_2(\cdot)$	continuous functions
μ	$= \frac{1}{r_{max}}$, inverse of the maximum allowable yaw rate
$\boldsymbol{\nu}$	linear and angular velocity vector
ξ	dimensionless damping coefficient
ξ_n	notch filter dimensionless damping coefficient
$\boldsymbol{\xi}$	integrating state

$\boldsymbol{\tau}$	forces and moments vector
	control input
τ_R	radiation-induced forces and moments
τ_D	damping forces and moments
τ_E	environmental forces and moments
ϕ	rotation about x-axis
ψ	rotation about z-axis
ω_0	dominant wave frequency
ω_c	cut-off frequency
Λ	damping matrix in the wave model
Σ_1, Σ_2	systems
Ω	matrix with eigenvalues in the wave model

Subscripts

b	bias model
	back
c	closed-loop
d	desired
e	error
f	front
i	degree of freedom ($i = 1, 2, 3$)
	sensor number ($i = 1, \ldots, 6$)
	thruster number ($i = 1, \ldots, 5$)
r, $\dot{r}$	surge-direction
ref	reference
u, $\dot{u}$	sway-direction
v, $\dot{v}$	yaw-direction
w	wave model
A	added mass/inertia
RB	rigid body

Chapter 1

Introduction

In marine applications, it is often necessary that a vessel maintains its position and orientation in the sea or follows a certain reference trajectory. Examples of such vessels are cable-layers, ice-breakers and offshore supply vessels. Moreover, nowadays freely floating oil drilling platforms are built, which can operate in seas where the water depth is too large for maintaining position merely by means of anchors.

1.1 Problem Formulation

These position and orientation keeping issues demand for the definition of a so-called dynamically positioned vessel (Fossen, 1994):

> *A dynamically positioned vessel is a vessel which maintains its position (fixed position or predetermined track) exclusively by means of active thrusters.*

A dynamic positioning (DP) system thus has to make sure that a vehicle maintains a specified position and orientation, unaffected by the disturbances acting upon it. In order to do so, proper counteracting forces have to attenuate these disturbances such that the positioning goal is achieved. Additionally, there are strict safety requirements upon a positioning system used in practice, due to the high risk for crew and equipment, especially in severe weather.

Currently, research on a phenomenon called parametric rolling is carried out at the Mechanics and Ocean Engineering section of the Mechanical Engineering department at the Technical University Hamburg-Harburg. This is a phenomenon, which occurs when large

container ships navigate on the sea while waves are overtaking the ship (a so-called following sea). Due to coupling between the ship motions in different directions, very strong rolling motions (rotation about an axis from aft to fore) can occur, which is called parametric rolling. Many container ships have lost containers due to this and this can even lead to capsizing. In order to investigate this phenomenon in a model setup, a floating body has to maintain its position and orientation relative to the waves by means of actively controlled thrusters. Due to the waves, an uncontrolled floating body would, however, attain an orientation where the waves come from either the port or starboard side (a so-called beam sea situation). A dynamic positioning control system will provide a solution to this problem as a fixed heading and position can be maintained. Therefore, the following problem definition is formulated for this project:

> *Design, analyse and test a dynamic positioning system for a floating body, such that a specific position and orientation relative to the waves can be maintained.*

1.2 Outline of the Report

In order to obtain a solution to the problem stated in the problem definition, a mathematical model of the ship in the experimental setup and a suitable positioning controller have to be designed.

For this purpose, first, a model of the ship and the environmental disturbances acting on it is derived in chapter 2.

Secondly, chapter 3 describes the design of a model-based observer of the ship and environment model. Moreover, a controller is designed based on the output of the observer.

Next, the experimental setup is discussed in chapter 4, where important properties of the experimental setup are discussed. Furthermore, the parameter values for the model are given.

In chapter 5, the implementation of the controller on the experimental setup is elucidated. Moreover, simulation and experimental results are discussed for a typical experiment.

Finally, conclusions are drawn and some recommendations for future research are made in chapter 6.

Chapter 2

Model for Dynamic Positioning

This chapter discusses the mathematical model, used to describe the dynamic positioning of the floating body. A general description of modelling of marine vehicles can be found in appendix A. In this chapter, first, the ship model will be discussed in section 2.1. Next, a suitable model for the environmental disturbances acting on the floating body is presented in section 2.2. Finally, the ship model and environment model are combined into the complete dynamic positioning model.

2.1 Dynamic Positioning Ship Model

2.1.1 Kinematics

The general motion of a marine vehicle is described by 6 degrees of freedom, using two coordinate frames; an earth-fixed reference frame, and a body-fixed frame (see appendix A.1 for details).

However, in the dynamic positioning problem, considered in this project, a surface ship has to maintain its position exclusively by means of active thrusters. Therefore, only motions in a horizontal plane, namely surge, sway and yaw, are considered, whereas the heave, roll and pitch motions are neglected. As a result, the position, velocity and force and moment vectors, as given in appendix A.1, reduce to the following:

$$\boldsymbol{\eta} = [x, y, \psi]^T; \qquad \boldsymbol{\nu} = [u, v, r]^T; \qquad \boldsymbol{\tau} = [X, Y, N]^T. \tag{2.1}$$

The kinematic relation (A.4) reduces to

$$\dot{\boldsymbol{\eta}} = \boldsymbol{J}(\boldsymbol{\eta})\boldsymbol{\nu} = \boldsymbol{J}(\psi)\boldsymbol{\nu}, \tag{2.2}$$

with rotation matrix

$$\boldsymbol{J}(\psi) = \begin{bmatrix} \cos(\psi) & -\sin(\psi) & 0 \\ \sin(\psi) & \cos(\psi) & 0 \\ 0 & 0 & 1 \end{bmatrix}. \tag{2.3}$$

Furthermore, in chapter 3, the time derivative $\dot{\boldsymbol{J}}$ of the transformation matrix will be needed. The expression for this is the following:

$$\dot{\boldsymbol{J}}(\psi) = \dot{\psi}\boldsymbol{S}\boldsymbol{J}(\psi) = r\boldsymbol{S}\boldsymbol{J}(\psi), \text{ with } \boldsymbol{S} = \begin{bmatrix} 0 & -1 & 0 \\ 1 & 0 & 0 \\ 0 & 0 & 0 \end{bmatrix}. \tag{2.4}$$

2.1.2 Dynamics

To describe the dynamics of the floating body, two important contributions are worthwhile mentioning. Namely, the dynamics consist of the rigid-body dynamics and the contribution of hydrodynamic forces and moments. The hydrodynamic forces and moments are included as two terms; as added mass and damping terms and as environmental disturbances. The latter will be discussed in section 2.2. A description of the rigid-body dynamics and the hydrodynamic forces and moments can be found in appendices A.2 and A.3, respectively.

The floating body, considered here is known to have xy (port–starboard) symmetry. The body-fixed coordinate origin is set to the centerline of the ship ($y_G = 0$). Moreover, it is common for slender surface ships to decouple the surge motion from the sway and yaw motion (see Fossen, 1994). These simplifications result in the following expressions for the rigid-body mass-matrix and the rigid-body matrix with coriolis and centripetal terms, respectively:

$$\boldsymbol{M}_{RB} = \begin{bmatrix} m & 0 & 0 \\ 0 & m & mx_G \\ 0 & mx_G & I_z \end{bmatrix}, \quad \boldsymbol{C}_{RB}(\boldsymbol{\nu}) = \begin{bmatrix} 0 & 0 & -m(x_G r + v) \\ 0 & 0 & mu \\ m(x_G r + v) & -mu & 0 \end{bmatrix}. \tag{2.5}$$

Here, m denotes the mass of the ship, I_z denotes the moment of inertia of the ship around its center of gravity for rotations in yaw-direction and x_G is the distance in x direction from the body-fixed coordinate system to the center of gravity of the ship.

Next, added mass and inertia have to be considered. Once again, the surge motion is decoupled from the sway and yaw motion. Furthermore, as stated in appendix A.3.1, the added mass coefficients are evaluated for zero frequency for positioned ships. The following

expressions result:

$$\boldsymbol{M}_A = \begin{bmatrix} -X_{\dot{u}} & 0 & 0 \\ 0 & -Y_{\dot{v}} & -Y_{\dot{r}} \\ 0 & -Y_{\dot{r}} & -N_{\dot{r}} \end{bmatrix}, \quad \boldsymbol{C}_A(\boldsymbol{\nu}) = \begin{bmatrix} 0 & 0 & Y_{\dot{v}}v + Y_{\dot{r}}r \\ 0 & 0 & -X_{\dot{u}}u \\ -Y_{\dot{v}}v - Y_{\dot{r}}r & X_{\dot{u}}u & 0 \end{bmatrix}, \tag{2.6}$$

where, for instance, the hydrodynamic added mass force Y_A in the sway direction due to an acceleration $\dot{r}$ in yaw direction can be found from $Y_A = Y_{\dot{r}}\dot{r}$. Note that the diagonal elements in $\boldsymbol{M}_A$ are positive by sign convention, which means that the diagonal added mass coefficients are negative themselves (for example $X_{\dot{u}} < 0$).

Moreover, for hydrodynamic damping of dynamically positioned ships, linearized damping is assumed. Here, once again, the surge motion is decoupled from the other two motions. The damping matrix is given by:

$$\boldsymbol{D}(\boldsymbol{\nu}) = \boldsymbol{D} = \begin{bmatrix} -X_u & 0 & 0 \\ 0 & -Y_v & -Y_r \\ 0 & -N_v & -N_r \end{bmatrix}. \tag{2.7}$$

Note, that the damping matrix does not necessarily have to be symmetric. Furthermore, the restoring forces and moments do not have to be taken into account for surface ships that are metacentric stable (see appendix A.3.3). As a result, the 3 DOF dynamic positioning version of the general equation of motion (equation (A.11) in appendix A.3) can be stated as:

$$\boldsymbol{M}\dot{\boldsymbol{\nu}} + \boldsymbol{C}(\boldsymbol{\nu})\boldsymbol{\nu} + \boldsymbol{D}\boldsymbol{\nu} = \boldsymbol{\tau}_E + \boldsymbol{\tau}, \tag{2.8}$$

where $\boldsymbol{M} = \boldsymbol{M}_{RB} + \boldsymbol{M}_A$ and $\boldsymbol{C}(\boldsymbol{\nu}) = \boldsymbol{C}_{RB}(\boldsymbol{\nu}) + \boldsymbol{C}_A(\boldsymbol{\nu})$ are given as:

$$\boldsymbol{M} = \begin{bmatrix} m - X_{\dot{u}} & 0 & 0 \\ 0 & m - Y_{\dot{v}} & mx_G - Y_{\dot{r}} \\ 0 & mx_G - Y_{\dot{r}} & I_z - N_{\dot{r}} \end{bmatrix}, \tag{2.9}$$

$$\boldsymbol{C}(\boldsymbol{\nu}) = \begin{bmatrix} 0 & 0 & -(m - Y_{\dot{v}})v - (mx_G - Y_{\dot{r}})r \\ 0 & 0 & (m - X_{\dot{u}})u \\ (m - Y_{\dot{v}})v + (mx_G - Y_{\dot{r}})r & -(m - X_{\dot{u}})u & 0 \end{bmatrix}. \tag{2.10}$$

It can be seen that the mass matrix is symmetric and positive definite ($\boldsymbol{M} = \boldsymbol{M}^T > 0$). Moreover, for dynamic positioning, the ship operates at very low velocities. Hence, an additional assumption is to neglect the term $\boldsymbol{C}(\boldsymbol{\nu})\boldsymbol{\nu}$, which is quadratic in the velocities.

2.2 Dynamic Positioning Environment Model

In the experimental setup, the environmental disturbances on the floating body consist of waves. In general, these disturbances are both additive and multiplicative to the equations of motion. Here, however, they are assumed to be only additive, such that the principle of superposition holds. In control systems design, it is common to split these additive disturbances into first-order wave disturbances (relatively high-frequent oscillatory motions) and second-order wave drift (see Fossen, 1994). A detailed treatment of these two disturbances is given in appendix A.4. Using this approach, the first-order wave disturbances are modelled by means of a linear wave approximation model and the second-order wave drift by means of a bias model.

2.2.1 First-Order Wave Disturbances

In analogy to the model in appendix A.4.1, for each DOF of the ship, a fourth-order wave model is used. This is given as a state-space description ($\boldsymbol{x}_w \in \mathbb{R}^{12}$ and $\boldsymbol{y} \in \mathbb{R}^3$):

$$\dot{\boldsymbol{x}}_w = \boldsymbol{A}_w \boldsymbol{x}_w + \boldsymbol{E}_w \boldsymbol{w}_w, \tag{2.11}$$

$$\boldsymbol{y}_w = \boldsymbol{C}_w \boldsymbol{x}_w, \tag{2.12}$$

$$\boldsymbol{A}_w = \begin{bmatrix} 0 & \boldsymbol{I} & 0 & 0 \\ -\boldsymbol{\Omega} & -\boldsymbol{\Lambda} & 0 & \boldsymbol{I} \\ 0 & 0 & 0 & \boldsymbol{I} \\ 0 & 0 & -\boldsymbol{\Omega} & -\boldsymbol{\Lambda} \end{bmatrix}, \quad \boldsymbol{E}_w = \begin{bmatrix} 0 \\ 0 \\ 0 \\ \boldsymbol{K}_w \end{bmatrix}, \quad \boldsymbol{C}_w = \begin{bmatrix} \boldsymbol{I} & 0 & 0 & 0 \end{bmatrix}. \tag{2.13}$$

$\boldsymbol{\Omega}$ and $\boldsymbol{\Lambda}$ are diagonal matrices containing terms with the dominant wave frequency and relative damping coefficients in x, y and ψ direction:

$$\boldsymbol{\Omega} = \begin{bmatrix} \omega_{01}^2 & 0 & 0 \\ 0 & \omega_{02}^2 & 0 \\ 0 & 0 & \omega_{03}^2 \end{bmatrix}, \quad \boldsymbol{\Lambda} = \begin{bmatrix} 2\xi_1\omega_{01} & 0 & 0 \\ 0 & 2\xi_2\omega_{02} & 0 \\ 0 & 0 & 2\xi_3\omega_{03} \end{bmatrix}. \tag{2.14}$$

Furthermore, $\boldsymbol{I}$ is the 3×3 identity matrix and $\boldsymbol{K}_w$ is a diagonal matrix containing the wave intensities k_{w1}, k_{w2} and k_{w3} in the three degrees of freedom. Note that the first-order wave disturbances do *not* directly appear in the equations of motion. Instead, the output (2.12) is added to the measured position and heading, as will become clear in the section 2.3.

2.2.2 Second-Order Wave Drift

For modelling the second-order drift forces by means of a bias model, the model from appendix A.4.2 can be used directly, with the difference that $\boldsymbol{b} \in \mathbb{R}^3$. This results in the following:

$$\dot{\boldsymbol{b}} = -\boldsymbol{T}_b^{-1}\boldsymbol{b} + \boldsymbol{E}_b\boldsymbol{w}_b, \tag{2.15}$$

were, $\boldsymbol{b}$ is a vector with bias forces and moments, $\boldsymbol{T}_b$ is a diagonal matrix with bias time constants T_{bi} $(i = 1, 2, 3)$ (typically chosen large), $\boldsymbol{w}_b$ is a vector of zero mean Gaussian white noise processes and $\boldsymbol{E}_b$ is a diagonal matrix scaling the amplitude of $\boldsymbol{w}_b$.

2.3 Complete Dynamic Positioning Model

By combining the ship and environment models, given in the previous two sections, the complete ship and environment model for dynamic positioning is obtained. The following results:

$$\begin{aligned}
\dot{\boldsymbol{x}}_w &= \boldsymbol{A}_w\boldsymbol{x}_w + \boldsymbol{E}_w\boldsymbol{w}_w, && (2.16)\\
\dot{\boldsymbol{\eta}} &= \boldsymbol{J}(\psi)\boldsymbol{\nu}, && (2.17)\\
\dot{\boldsymbol{b}} &= -\boldsymbol{T}_b^{-1}\boldsymbol{b} + \boldsymbol{E}_b\boldsymbol{w}_b, && (2.18)\\
\boldsymbol{M}\dot{\boldsymbol{\nu}} &= -\boldsymbol{D}\boldsymbol{\nu} + \boldsymbol{J}^T(\psi)\boldsymbol{b} + \boldsymbol{\tau}, && (2.19)\\
\boldsymbol{y} &= \boldsymbol{\eta} + \boldsymbol{y}_w + \boldsymbol{v} = \boldsymbol{\eta} + \boldsymbol{C}_w\boldsymbol{x}_w + \boldsymbol{v}. && (2.20)
\end{aligned}$$

Equations (2.16)–(2.20) form a state-space model for the ship and the wave environment with $\boldsymbol{x}_w \in \mathbb{R}^{12}$ and $\boldsymbol{\eta}, \boldsymbol{b}, \boldsymbol{\nu} \in \mathbb{R}^3$. This model has quite a linear nature, apart from the rotation matrix $\boldsymbol{J}(\psi)$. As can be seen in equation (2.20), the output of the model contains the additive first order wave disturbances (the term $\boldsymbol{C}_w\boldsymbol{x}_w$). Furthermore, a measurement noise term $\boldsymbol{v}$ is added here. Based on this output, an observer and controller will be designed in chapter 3. The control $\boldsymbol{\tau}$ depends on the layout of the thrusters in the ship, which will be discussed in chapter 4.

Chapter 3

Observer and Controller Design

In this chapter, the design of the dynamic positioning system is discussed. In order to arrive at the final controller, firstly, the general idea behind the controller will be discussed in section 3.1. Here, it will become clear that an observer is needed and it is illuminated what properties are necessary for a dynamic positioning system. Next, the derivation of the observer and the controller are discussed in section 3.2 and 3.3, respectively. Finally, the complete dynamic positioning system is given in section 3.4.

3.1 General Idea

As stated in the section 1.1, a dynamic positioning (DP) system has to make sure that a ship maintains its position and heading actively by means of thrusters. In most cases, however, only position measurements are available. Consequently, filtering and state estimation are important features of a DP system, as will be explained next. Namely, the velocities of the vessel must be calculated from the position and heading measurements using some kind of state estimator. Unfortunately, the measurements are corrupted with sensor noise as well as coloured noise due to wind, waves and currents. The dynamic positioning system should only counteract the slowly varying disturbances (second order wave drift) to avoid unnecessary wear and tear in the propulsion equipment. Otherwise, excessive thruster modulation would be required to compensate for the first order wave disturbances. For this purpose, so-called wave-filtering techniques are applied, where the position and heading measurements are separated in low-frequent (drift) and high-frequent (wave disturbance) components.

Several control strategies are available to achieve the aforementioned properties. Firstly,

Kalman filtering techniques can be applied to separate the high-frequent first order wave disturbances from the low-frequent wave drift, such that only the latter can be used for feedback (see for example Fung and Grimble, 1983). Alternatively, observer-based dynamic positioning control is possible, in which a non-linear observer is used to estimate the low frequent wave drift together with the vessel's velocities. Subsequently, the observer outputs are used for positioning control. This method is, for instance, described in Fossen and Strand (1999), Strand (1999) and Lindegaard (2003) and will be explained in the next sections.

3.2 Observer Design

In order to obtain estimates of the low-frequent position components, an observer for the model, described in section 2.3, is derived in this section. This observer has to reconstruct the low-frequent component $\boldsymbol{\eta}$ from the measurement equation $\boldsymbol{y} = \boldsymbol{\eta} + \boldsymbol{y}_w + \boldsymbol{v}$ (see equation (2.20)). Additionally, an estimate of the low-frequent velocity $\boldsymbol{\nu}$ has to be obtained. To achieve these properties of the observer, the wave model will also be included, such that the observer will act as a notch-filter in the frequency range of the wave disturbances.

3.2.1 Assumptions

In the design of the observer, some assumptions have to be made with respect to the Lyapunov stability analysis. These assumptions are the following:

- $\boldsymbol{M} = \boldsymbol{M}^T > 0$. The mass matrix of the ship is assumed to be symmetric and positive definite. This is true for surface ships with port-starboard symmetry for low velocities, as explained in section 2.1.2. Furthermore, it is assumed that the added mass terms are independent of the wave-frequency ($\dot{\boldsymbol{M}} = \boldsymbol{0}$); a condition which is also satisfied for the DP problem (see appendix A.3.1).

- $\boldsymbol{w}_w = \boldsymbol{w}_b = 0$. The wave disturbance model and the bias model are driven by zero-mean Gaussian white noise. These terms are not included in the observer model and the Lyapunov stability analysis since the observer model is driven by the estimation error instead (see Fossen and Strand, 1999).

- $\boldsymbol{v} = 0$. The zero-mean Gaussian white measurement noise is not included in the Lyapunov analysis since this term is considered to be negligible compared to the first order wave disturbances $\boldsymbol{\eta}_w$.

- $\boldsymbol{J}(\boldsymbol{\eta}) = \boldsymbol{J}(\boldsymbol{y})$ or $\boldsymbol{J}(\psi) = \boldsymbol{J}(\psi + \psi_w)$. The amplitude of the first-order wave-induced yaw-angle disturbance is assumed to be small. Namely, ψ_w will be less than 1° for normal sea conditions and less than 5° for extreme weather situations (Strand, 1999).

By applying these assumptions to the DP ship and environment model (2.16)–(2.20), the following system model results:

$$\dot{\boldsymbol{x}}_w = \boldsymbol{A}_w \boldsymbol{x}_w, \tag{3.1}$$

$$\dot{\boldsymbol{\eta}} = \boldsymbol{J}(\psi)\boldsymbol{\nu}, \tag{3.2}$$

$$\dot{\boldsymbol{b}} = -\boldsymbol{T}_b^{-1}\boldsymbol{b}, \tag{3.3}$$

$$\boldsymbol{M}\dot{\boldsymbol{\nu}} = -\boldsymbol{D}\boldsymbol{\nu} + \boldsymbol{J}^T(\psi)\boldsymbol{b} + \boldsymbol{\tau}, \tag{3.4}$$

$$\boldsymbol{y} = \boldsymbol{\eta} + \boldsymbol{C}_w \boldsymbol{x}_w. \tag{3.5}$$

Furthermore, for notational convenience, equations (3.1), (3.2) and (3.5) are combined and written in state-space form as:

$$\dot{\boldsymbol{x}}_0 = \boldsymbol{A}_0 \boldsymbol{x}_0 + \boldsymbol{B}_0 \boldsymbol{J}(\psi)\boldsymbol{\nu}, \tag{3.6}$$

$$\boldsymbol{y} = \boldsymbol{C}_0 \boldsymbol{x}_0, \tag{3.7}$$

where $\boldsymbol{x}_0 = [\boldsymbol{x}_w^T, \boldsymbol{\eta}^T]^T$ and:

$$\boldsymbol{A}_0 = \begin{bmatrix} \boldsymbol{A}_w & \boldsymbol{0} \\ \boldsymbol{0} & \boldsymbol{0} \end{bmatrix}, \qquad \boldsymbol{B}_0 = \begin{bmatrix} \boldsymbol{0} \\ \boldsymbol{I} \end{bmatrix}, \qquad \boldsymbol{C}_0 = \begin{bmatrix} \boldsymbol{C}_w & \boldsymbol{I} \end{bmatrix}. \tag{3.8}$$

3.2.2 Non-linear Observer

A full-state non-linear observer, copying the dynamics (3.1)–(3.5) is the following (see Fossen and Strand, 1999):

$$\dot{\hat{\boldsymbol{x}}}_w = \boldsymbol{A}_w \hat{\boldsymbol{x}}_w + \boldsymbol{K}_1 \tilde{\boldsymbol{y}}, \tag{3.9}$$

$$\dot{\hat{\boldsymbol{\eta}}} = \boldsymbol{J}(\psi)\hat{\boldsymbol{\nu}} + \boldsymbol{K}_2 \tilde{\boldsymbol{y}}, \tag{3.10}$$

$$\dot{\hat{\boldsymbol{b}}} = -\boldsymbol{T}_b^{-1}\hat{\boldsymbol{b}} + \frac{1}{\gamma}\boldsymbol{K}_3 \tilde{\boldsymbol{y}}, \tag{3.11}$$

$$\boldsymbol{M}\dot{\hat{\boldsymbol{\nu}}} = -\boldsymbol{D}\hat{\boldsymbol{\nu}} + \boldsymbol{J}^T(\psi)\hat{\boldsymbol{b}} + \boldsymbol{\tau} + \frac{1}{\gamma}\boldsymbol{J}^T(\psi)\boldsymbol{K}_4 \tilde{\boldsymbol{y}}, \tag{3.12}$$

$$\hat{\boldsymbol{y}} = \hat{\boldsymbol{\eta}} + \boldsymbol{C}_w \hat{\boldsymbol{x}}_w. \tag{3.13}$$

Here, $\tilde{\boldsymbol{y}} = \boldsymbol{y} - \hat{\boldsymbol{y}}$ is the innovation error and $\boldsymbol{K}_1 \in \mathbb{R}^{12\times 3}$ and $\boldsymbol{K}_2, \boldsymbol{K}_3, \boldsymbol{K}_4 \in \mathbb{R}^{3\times 3}$ are observer gain matrices to be determined later. $\gamma > 0$ is an additional scalar tuning parameter. The general structure of the observer can be seen in a block diagram representation in figure 3.1.

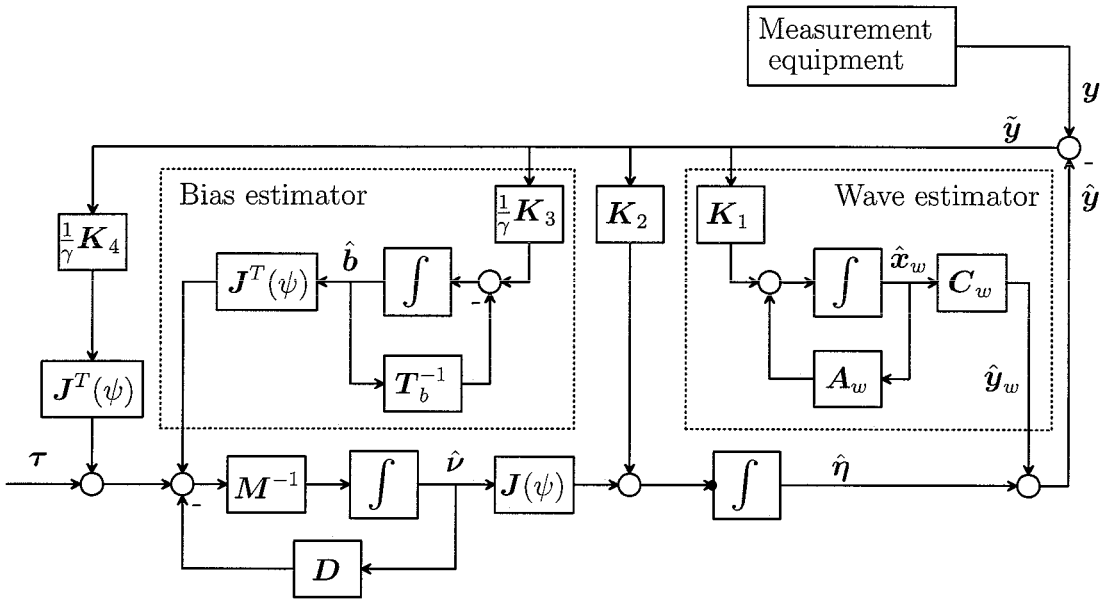

Figure 3.1: Schematic block diagram representation of the observer.

Next, a similar notation as in (3.6) and (3.7) is obtained by writing (3.9), (3.10) and (3.13) in state-space form:

$$\dot{\hat{\boldsymbol{x}}}_0 = \boldsymbol{A}_0\hat{\boldsymbol{x}}_0 + \boldsymbol{B}_0\boldsymbol{J}(\psi)\hat{\boldsymbol{\nu}} + \boldsymbol{K}\tilde{\boldsymbol{y}}, \tag{3.14}$$

$$\hat{\boldsymbol{y}} = \boldsymbol{C}_0\hat{\boldsymbol{x}}_0, \tag{3.15}$$

where $\hat{\boldsymbol{x}}_0 = [\hat{\boldsymbol{x}}_w^T, \hat{\boldsymbol{\eta}}^T]^T$ and:

$$\boldsymbol{K} = \begin{bmatrix} \boldsymbol{K}_1 \\ \boldsymbol{K}_2 \end{bmatrix}. \tag{3.16}$$

Matrices $\boldsymbol{A}_0$, $\boldsymbol{B}_0$ and $\boldsymbol{C}_0$ are defined as in (3.8).

In order to obtain expressions for the observer error dynamics, the estimation errors are defined as $\tilde{\boldsymbol{\nu}} = \boldsymbol{\nu} - \hat{\boldsymbol{\nu}}$, $\tilde{\boldsymbol{b}} = \boldsymbol{b} - \hat{\boldsymbol{b}}$ and $\tilde{\boldsymbol{x}}_0 = \boldsymbol{x}_0 - \hat{\boldsymbol{x}}_0$. Hence, the error dynamics can be written as:

$$\dot{\tilde{\boldsymbol{x}}}_0 = (\boldsymbol{A}_0 - \boldsymbol{K}\boldsymbol{C}_0)\tilde{\boldsymbol{x}}_0 + \boldsymbol{B}_0\boldsymbol{J}(\psi)\tilde{\boldsymbol{\nu}}, \tag{3.17}$$

$$\dot{\tilde{\boldsymbol{b}}} = -\boldsymbol{T}_b^{-1}\tilde{\boldsymbol{b}} - \frac{1}{\gamma}\boldsymbol{K}_3\tilde{\boldsymbol{y}}, \tag{3.18}$$

$$\boldsymbol{M}\dot{\tilde{\boldsymbol{\nu}}} = -\boldsymbol{D}\tilde{\boldsymbol{\nu}} + \boldsymbol{J}^T(\psi)\tilde{\boldsymbol{b}} - \frac{1}{\gamma}\boldsymbol{J}^T(\psi)\boldsymbol{K}_4\tilde{\boldsymbol{y}}, \tag{3.19}$$

where use is made of the fact that $\tilde{\boldsymbol{y}} = \boldsymbol{C}_0\tilde{\boldsymbol{x}}_0$. Next, a new output is defined, consisting of a linear combination of the estimation errors:

$$\tilde{\boldsymbol{z}} = \boldsymbol{K}_4\tilde{\boldsymbol{y}} - \gamma\tilde{\boldsymbol{b}}, \tag{3.20}$$

and a vector $\tilde{\boldsymbol{x}}$ is defined as

$$\tilde{\boldsymbol{x}} = \begin{bmatrix} \tilde{\boldsymbol{x}}_0 \\ \tilde{\boldsymbol{b}} \end{bmatrix}, \tag{3.21}$$

such that (3.17)–(3.20) can be written in compact form:

$$\dot{\tilde{\boldsymbol{x}}} = \boldsymbol{A}\tilde{\boldsymbol{x}} + \boldsymbol{B}\boldsymbol{J}(\psi)\tilde{\boldsymbol{\nu}}, \tag{3.22}$$

$$\tilde{\boldsymbol{z}} = \boldsymbol{C}\tilde{\boldsymbol{x}}, \tag{3.23}$$

$$\boldsymbol{M}\dot{\tilde{\boldsymbol{\nu}}} = -\boldsymbol{D}\tilde{\boldsymbol{\nu}} - \frac{1}{\gamma}\boldsymbol{J}^T(\psi)\tilde{\boldsymbol{z}}. \tag{3.24}$$

where

$$\boldsymbol{A} = \begin{bmatrix} \boldsymbol{A}_0 - \boldsymbol{K}\boldsymbol{C}_0 & \boldsymbol{0} \\ -\frac{1}{\gamma}\boldsymbol{K}_3\boldsymbol{C}_0 & -\boldsymbol{T}_b^{-1} \end{bmatrix}, \quad \boldsymbol{B} = \begin{bmatrix} \boldsymbol{B}_0 \\ \boldsymbol{0} \end{bmatrix}, \quad \boldsymbol{C} = \begin{bmatrix} \boldsymbol{K}_4\boldsymbol{C}_0 & -\gamma\boldsymbol{I} \end{bmatrix}. \tag{3.25}$$

3.2.3 Stability Analysis

In the following, the stability of the observer will be proven. The error dynamics (3.22)–(3.24) are depicted in block diagram form in figure 3.2, where two new error terms are defined as:

$$\boldsymbol{\varepsilon}_z = -\boldsymbol{J}^T(\psi)\tilde{\boldsymbol{z}}, \qquad \boldsymbol{\varepsilon}_\nu = \boldsymbol{J}(\psi)\tilde{\boldsymbol{\nu}}. \tag{3.26}$$

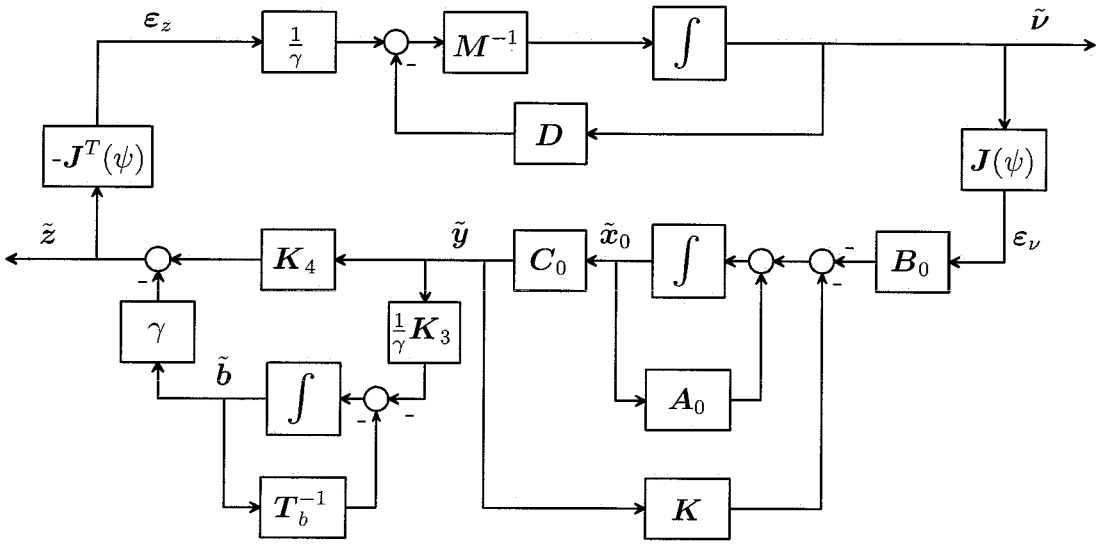

Figure 3.2: Schematic block-diagram showing the dynamics of the position/bias and velocity estimation errors.

Hence, the observer error dynamics consist of two linear sections, interconnected through the bounded transformation matrix $\boldsymbol{J}(\psi)$.

Next, the stability of the complete observer is assessed. This is summarised in the following theorem (see Fossen and Strand, 1999):

Theorem 3.1 (Global Asymptotic Stability of the Observer)
Under the assumptions stated in section 3.2.1, the non-linear observer given by equations (3.9)– (3.13) *is globally asymptotically stable.*

Proof. The proof of Theorem 3.1 consists of a tuning procedure for the observer gain matrices and a Lyapunov analysis. First, the tuning procedure is described.

To assess the stability of the error dynamics (3.22)–(3.24), Lemma 3.1 is needed:

Lemma 3.1 (Kalman-Yakubovich-Popov (KYP) Lemma)
Let $Z(s) = \mathcal{C}(sI - \mathcal{A})^{-1}\mathcal{B}$ be an $n \times n$ transfer function matrix, where $\mathcal{A}$ is Hurwitz, $(\mathcal{A}, \mathcal{B})$ is controllable, and $(\mathcal{A}, \mathcal{C})$ is observable. Then, $Z(s)$ is strictly positive real (SPR) if and only if there exist positive definite matrices $\mathcal{P} = \mathcal{P}^T$ and $\mathcal{Q} = \mathcal{Q}^T$, such that (Khalil, 1996):

$$\mathcal{P}\mathcal{A} + \mathcal{A}^T\mathcal{P} = -\mathcal{Q}, \tag{3.27}$$

$$\mathcal{B}^T\mathcal{P} = \mathcal{C}. \tag{3.28}$$

For a $\gamma > 0$, and for the observer gain matrices with the following structure:

$$\boldsymbol{K}_1 = \begin{bmatrix} k_{11} & 0 & 0 \\ 0 & k_{12} & 0 \\ 0 & 0 & k_{13} \\ k_{21} & 0 & 0 \\ 0 & k_{22} & 0 \\ 0 & 0 & k_{23} \\ k_{31} & 0 & 0 \\ 0 & k_{32} & 0 \\ 0 & 0 & k_{33} \\ k_{41} & 0 & 0 \\ 0 & k_{42} & 0 \\ 0 & 0 & k_{43} \end{bmatrix}, \quad \boldsymbol{K}_2 = \begin{bmatrix} k_{51} & 0 & 0 \\ 0 & k_{52} & 0 \\ 0 & 0 & k_{53} \end{bmatrix}, \quad \boldsymbol{K}_3 = \begin{bmatrix} k_{61} & 0 & 0 \\ 0 & k_{62} & 0 \\ 0 & 0 & k_{63} \end{bmatrix}, \quad \boldsymbol{K}_4 = \begin{bmatrix} k_{71} & 0 & 0 \\ 0 & k_{72} & 0 \\ 0 & 0 & k_{73} \end{bmatrix}, \tag{3.29}$$

the elements $k_{ji} > 0$ of the observer gain matrices can be chosen such that the mapping $\boldsymbol{\varepsilon}_\nu \mapsto \tilde{\boldsymbol{z}}$ satisfies the KYP lemma. This mapping consists of matrices $\boldsymbol{A}, \boldsymbol{B}$ and $\boldsymbol{C}$, given in equation (3.25). Because of the diagonal-like structure of the observer gain matrices, the mapping $\boldsymbol{\varepsilon}_\nu \mapsto \tilde{\boldsymbol{z}}$ can be described by three decoupled transfer functions. Furthermore, this mapping can be written as two consecutive mappings: $\boldsymbol{\varepsilon}_\nu \mapsto \tilde{\boldsymbol{y}}$ and $\tilde{\boldsymbol{y}} \mapsto \tilde{\boldsymbol{z}}$, each with

their own diagonal transfer function matrix. In the frequency domain, this can be written as:

$$\tilde{\boldsymbol{z}}(s) = \boldsymbol{H}_{\boldsymbol{\varepsilon}_\nu,\tilde{\boldsymbol{z}}}(s)\boldsymbol{\varepsilon}_\nu(s), \quad \text{with} \quad \boldsymbol{H}_{\boldsymbol{\varepsilon}_\nu,\tilde{\boldsymbol{z}}}(s) = \boldsymbol{H}_{\boldsymbol{\varepsilon}_\nu,\tilde{\boldsymbol{y}}}(s)\boldsymbol{H}_{\tilde{\boldsymbol{y}},\tilde{\boldsymbol{z}}}(s), \tag{3.30}$$

where the transfer function matrices $\boldsymbol{H}_{\boldsymbol{\varepsilon}_\nu,\tilde{\boldsymbol{y}}}(s)$ and $\boldsymbol{H}_{\tilde{\boldsymbol{y}},\tilde{\boldsymbol{z}}}(s)$ are computed from (3.17), (3.18) and (3.20) (using $\tilde{\boldsymbol{y}} = \boldsymbol{C}_0\tilde{\boldsymbol{x}}_0$) are found to equal:

$$\boldsymbol{H}_{\boldsymbol{\varepsilon}_\nu,\tilde{\boldsymbol{y}}}(s) = \boldsymbol{C}_0(s\boldsymbol{I} - \boldsymbol{A}_0 + \boldsymbol{K}\boldsymbol{C}_0)^{-1}\boldsymbol{B}_0, \tag{3.31}$$

$$\boldsymbol{H}_{\tilde{\boldsymbol{y}},\tilde{\boldsymbol{z}}}(s) = \boldsymbol{K}_4 + (s\boldsymbol{I} + \boldsymbol{T}_b^{-1})^{-1}\boldsymbol{K}_3. \tag{3.32}$$

Consequently, the diagonal component i $(i = 1, 2, 3)$ of these transfer function matrices can be written as:

$$h^i_{\boldsymbol{\varepsilon}_\nu,\tilde{\boldsymbol{y}}}(s) = \frac{(s^2 + 2\xi_i\omega_{0i}s + \omega_{0i}^2)^2}{s^5 + a_{4i}s^4 + a_{3i}s^3 + a_{2i}s^2 + a_{1i}s + a_{0i}}, \tag{3.33}$$

$$h^i_{\tilde{\boldsymbol{y}},\tilde{\boldsymbol{z}}}(s) = k_{7i}\frac{s + \left(\frac{1}{T_{bi}} + \frac{k_{6i}}{k_{7i}}\right)}{s + \frac{1}{T_{bi}}}, \tag{3.34}$$

where the coefficients in (3.33) are given by:

$$a_{0i} = k_{5i}\omega_{0i}^4, \tag{3.35}$$

$$a_{1i} = 2k_{1i}\xi_i\omega_{0i}^3 + k_{2i}\omega_{0i}^2 - k_{3i}\omega_{0i}^2 + 4k_{5i}\xi_i\omega_{0i}^3 + \omega_{0i}^4, \tag{3.36}$$

$$a_{2i} = k_{1i}\omega_{0i}^2(4\xi_i^2 + 1) + 2k_{2i}\xi_i\omega_{0i} + k_{4i} + 2k_{5i}\omega_{0i}^2(2\xi_i^2 + 1) + 4\xi_i\omega_{0i}^3, \tag{3.37}$$

$$a_{3i} = 4k_{1i}\xi_i\omega_{0i} + k_{2i} + 4k_{5i}\xi_i\omega_{0i} + 2\omega_{0i}^2(2\xi_i^2 + 1), \tag{3.38}$$

$$a_{4i} = k_{1i} + k_{5i} + 4\xi_i\omega_{0i}. \tag{3.39}$$

In order to obtain the desired notch-filter effect of the observer, a desired shape of transfer function $h^i_{\boldsymbol{\varepsilon}_\nu,\tilde{\boldsymbol{y}}}(s)$ $(i = 1, 2, 3)$ is specified as a double notch filter in series with a low-pass filter:

$$h^i_{\boldsymbol{\varepsilon}_\nu,\tilde{\boldsymbol{y}}}(s) = \frac{(s^2 + 2\xi_i\omega_{0i}s + \omega_{0i}^2)^2}{(s^2 + 2\xi_{ni}\omega_{0i}s + \omega_{0i}^2)^2(s + \omega_{ci})}. \tag{3.40}$$

Here, $\xi_{ni} > \xi_i$ determines the notch depth and ω_{ci} determines the cut-off frequency of the filter. Note that, in general, this cut-off frequency is higher than the dominating wave frequency as the latter typically lies close to the desired bandwidth of the DP system.

The filter gains in matrices $\boldsymbol{K}_1$ and $\boldsymbol{K}_2$ can be found by equating (3.33) and (3.40), which gives the following expressions:

$$k_{1i} = 4\omega_{0i}(\xi_{ni} - \xi_i), \tag{3.41}$$

$$k_{2i} = -4\omega_{0i}(\xi_{ni} - \xi_i)(3\xi_i\omega_{0i} - \xi_{ni}\omega_{0i} - \omega_{ci}), \tag{3.42}$$

$$k_{3i} = 4\omega_{0i}^2(\xi_{ni} - \xi_i)^2, \tag{3.43}$$

$$k_{4i} = -4\omega_{0i}^2(\xi_{ni} - \xi_i)^2(2\xi_i\omega_{0i} - \omega_{ci}), \tag{3.44}$$

$$k_{5i} = \omega_{ci}. \tag{3.45}$$

In order to meet the SPR-requirement (Lemma 3.1), there are some restrictions in selecting for example ξ_{ni} and the gain in matrices $\boldsymbol{K}_3$ and $\boldsymbol{K}_4$. Namely, the three decoupled transfer functions $h^i_{\boldsymbol{\varepsilon}_\nu,\tilde{\boldsymbol{z}}}(s)$ $(i = 1,2,3)$ all have to have their phase between $-90°$ and $+90°$ to satisfy the KYP lemma (stated otherwise, their Nyquist plot has to lie completely in the right complex half-plane). By applying the following tuning rules for T_{bi}, k_{6i} and k_{7i}, this requirement can easily be met (Fossen and Strand, 1999):

$$\frac{1}{T_{bi}} < \frac{k_{6i}}{k_{7i}} < \omega_{0i} < \omega_{ci}, \qquad (i = 1,2,3). \tag{3.46}$$

An example of the complete transfer function $h^i_{\boldsymbol{\varepsilon}_\nu,\tilde{\boldsymbol{z}}}(s)$, with properly selected filter gains, is depicted in figure 3.3. The notch effect of the observer can clearly be seen here.

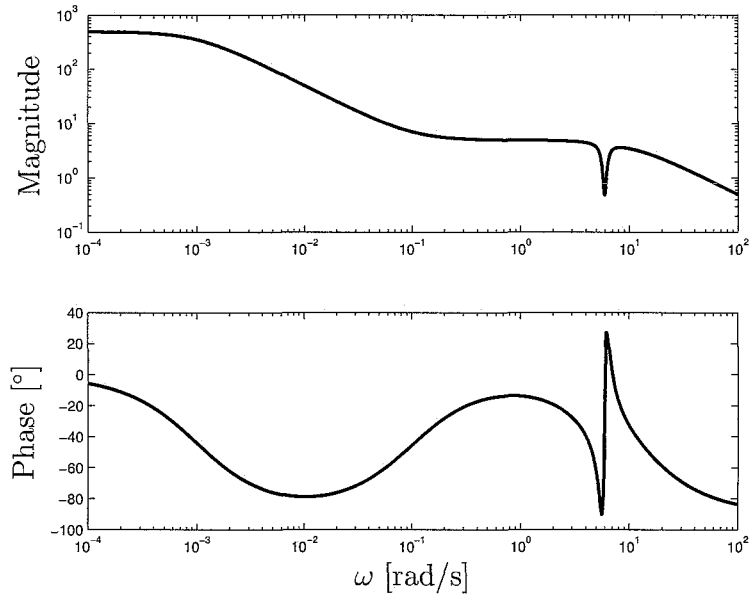

Figure 3.3: Example of the observer transfer function in yaw-direction (see also section 5.2.1).

However, the transfer function contains a relatively narrow notch, which indicates that the observer will not be robust for changes in wave frequency. As a solution to this problem, the observer could be made adaptive to the wave frequency, as is done in Strand (1999).

Next, the stability of the observer (3.9)–(3.13) is proven by Lyapunov analysis. Consider the following positive definite and radially unbounded candidate Lyapunov function:

$$V = \gamma \tilde{\boldsymbol{\nu}}^T \boldsymbol{M} \tilde{\boldsymbol{\nu}} + \tilde{\boldsymbol{x}}^T \boldsymbol{P} \tilde{\boldsymbol{x}}. \tag{3.47}$$

As required for this Lyapunov function, $V = 0$ for $\tilde{\boldsymbol{\nu}}, \tilde{\boldsymbol{x}} = \boldsymbol{0}$ and $V > 0$ for $\tilde{\boldsymbol{\nu}}, \tilde{\boldsymbol{x}} \neq \boldsymbol{0}$. Time differentiation of (3.47) and applying the assumptions stated in section 3.2.1 gives the following:

$$\dot{V} = \gamma \dot{\tilde{\boldsymbol{\nu}}}^T \boldsymbol{M} \tilde{\boldsymbol{\nu}} + \gamma \tilde{\boldsymbol{\nu}}^T \boldsymbol{M} \dot{\tilde{\boldsymbol{\nu}}} + \dot{\tilde{\boldsymbol{x}}}^T \boldsymbol{P} \tilde{\boldsymbol{x}} + \tilde{\boldsymbol{x}}^T \boldsymbol{P} \dot{\tilde{\boldsymbol{x}}}. \tag{3.48}$$

By using equation (3.22) and (3.24), this can be rewritten as:

$$\begin{aligned}\dot{V} &= -\gamma\tilde{\boldsymbol{\nu}}^T(\boldsymbol{D}^T+\boldsymbol{D})\tilde{\boldsymbol{\nu}}+\tilde{\boldsymbol{x}}^T(\boldsymbol{A}^T\boldsymbol{P}+\boldsymbol{P}\boldsymbol{A})\tilde{\boldsymbol{x}} \\ &\quad -2\tilde{\boldsymbol{\nu}}^T\boldsymbol{J}^T(\psi)\tilde{\boldsymbol{z}}+2\tilde{\boldsymbol{\nu}}^T\boldsymbol{J}^T(\psi)\boldsymbol{B}^T\boldsymbol{P}\tilde{\boldsymbol{x}}. \end{aligned} \tag{3.49}$$

Furthermore, as the system (3.22)–(3.23) satisfies the KYP Lemma, $\boldsymbol{A}^T\boldsymbol{P}+\boldsymbol{P}\boldsymbol{A}=-\boldsymbol{Q}$ and $\boldsymbol{B}^T\boldsymbol{P}=\boldsymbol{C}$. Additionally, it is used that $\tilde{\boldsymbol{z}}=\boldsymbol{C}\tilde{\boldsymbol{x}}$. Hence (3.49) simplifies to:

$$\dot{V}=-\gamma\tilde{\boldsymbol{\nu}}^T(\boldsymbol{D}^T+\boldsymbol{D})\tilde{\boldsymbol{\nu}}-\tilde{\boldsymbol{x}}^T\boldsymbol{Q}\tilde{\boldsymbol{x}}, \tag{3.50}$$

which is zero for $\tilde{\boldsymbol{\nu}},\tilde{\boldsymbol{x}}=\boldsymbol{0}$ and negative definite. As a result, $\tilde{\boldsymbol{\nu}}$ and $\tilde{\boldsymbol{x}}=[\tilde{\boldsymbol{x}}_w^T,\tilde{\boldsymbol{\eta}}^T,\tilde{\boldsymbol{b}}^T]^T$ converge asymptotically to zero, which completes the proof. □

3.3 Controller Design

Next, the derivation of a non-linear PID-like position controller for the system without observer is discussed (Lindegaard and Fossen, 2003; Lindegaard, 2003). The controller will be linear in the sense that the PID terms are linearly bounded in the error variables. The non-linearity comes from the fact that the kinematics are included in the design.

3.3.1 Controllability

Firstly, it has to be determined whether the system for which the controller is designed is controllable or not. The ship dynamics, without wave disturbances and bias model, are given in equation (2.17) and (2.19) and are stated here again, for convenience:

$$\dot{\boldsymbol{\eta}} = \boldsymbol{J}(\psi)\boldsymbol{\nu}, \tag{3.51}$$

$$\boldsymbol{M}\dot{\boldsymbol{\nu}} = -\boldsymbol{D}\boldsymbol{\nu}+\boldsymbol{\tau}. \tag{3.52}$$

Controllability can be illustrated by considering the system for a fixed heading angle, for instance $\psi=0$, which results in a linear system:

$$\begin{bmatrix}\dot{\boldsymbol{\eta}}\\ \dot{\boldsymbol{\nu}}\end{bmatrix}=\begin{bmatrix}\boldsymbol{0} & \boldsymbol{I}\\ \boldsymbol{0} & -\boldsymbol{M}^{-1}\boldsymbol{D}\end{bmatrix}\begin{bmatrix}\boldsymbol{\eta}\\ \boldsymbol{\nu}\end{bmatrix}+\begin{bmatrix}\boldsymbol{0}\\ \boldsymbol{M}^{-1}\end{bmatrix}\boldsymbol{\tau}. \tag{3.53}$$

This linear system is controllable. Furthermore, $\boldsymbol{J}(\psi)$ can be evaluated for any $\psi\in[0,2\pi]$ without becoming singular. Moreover, for a time-varying signal $\psi(t)$, also a controllable system results, as $\boldsymbol{J}(\psi(t))$ maintains full rank. Hence, for arbitrary $\psi(t)$, a controllable system is obtained, which implies that (3.51)–(3.52) is controllable.

3.3.2 Controller

In order to derive a control law for the system (3.51)–(3.52), the desired positions, velocities and accelerations are specified as $\boldsymbol{\eta}_d$, $\boldsymbol{\nu}_d$ and $\dot{\boldsymbol{\nu}}_d$, respectively. The general tracking case is considered here, although $\boldsymbol{\nu}_d = \dot{\boldsymbol{\nu}}_d = 0$ for dynamic positioning. This yields the following expressions for the position and velocity errors:

$$\boldsymbol{\eta}_e = \boldsymbol{\eta} - \boldsymbol{\eta}_d, \qquad \boldsymbol{\nu}_e = \boldsymbol{\nu} - \boldsymbol{\nu}_d. \tag{3.54}$$

Next, the following PID-like tracking control law is proposed (see Lindegaard and Fossen, 2003), where the integrating action is obtained from an additional state $\boldsymbol{\xi}$:

$$\dot{\boldsymbol{\xi}} = \boldsymbol{\eta}_e, \tag{3.55}$$

$$\boldsymbol{\tau} = -\boldsymbol{M}\left(\boldsymbol{K}_i\boldsymbol{J}^T(\psi)\boldsymbol{\xi} + \boldsymbol{K}_p\boldsymbol{J}^T(\psi)\boldsymbol{\eta}_e + \boldsymbol{K}_d\boldsymbol{\nu}_e\right) + \boldsymbol{D}\boldsymbol{\nu}_d + \boldsymbol{M}\dot{\boldsymbol{\nu}}_d. \tag{3.56}$$

Here, matrices $\boldsymbol{K}_p$, $\boldsymbol{K}_i$, $\boldsymbol{K}_d \in \mathbb{R}^{3\times 3}$ are the proportional, integral and derivative gain matrices, respectively. Note that $\boldsymbol{K}_i$ and $\boldsymbol{K}_p$ are put to the left of the rotation matrix $\boldsymbol{J}^T(\psi)$, which makes them body-fixed gains, independent of the heading of the ship. Furthermore, the last two terms in (3.56) are feedforward terms. When the reference trajectory is prescribed such that $\dot{\boldsymbol{\eta}}_d = \boldsymbol{J}(\psi)\boldsymbol{\nu}_d$, that is, the reference is consistent with the kinematics of the ship model, the control law can be inserted in (3.52), which yields the following closed-loop system:

$$\dot{\boldsymbol{\xi}} = \boldsymbol{\eta}_e, \tag{3.57}$$

$$\dot{\boldsymbol{\eta}}_e = \boldsymbol{J}(\psi)\boldsymbol{\nu}_e, \tag{3.58}$$

$$\boldsymbol{M}\dot{\boldsymbol{\nu}}_e = -(\boldsymbol{D} + \boldsymbol{M}\boldsymbol{K}_d)\boldsymbol{\nu}_e - \boldsymbol{M}\boldsymbol{K}_i\boldsymbol{J}^T(\psi)\boldsymbol{\xi}_e - \boldsymbol{M}\boldsymbol{K}_p\boldsymbol{J}^T(\psi)\boldsymbol{\eta}_e. \tag{3.59}$$

3.3.3 Stability Analysis

By defining $\boldsymbol{q} = [\boldsymbol{\xi}^T, \boldsymbol{\eta}_e^T, \boldsymbol{\nu}_e^T]^T$, the closed-loop system (3.57)–(3.59) can be written in state-space form as:

$$\dot{\boldsymbol{q}} = \boldsymbol{T}^T(\psi)\boldsymbol{A}_c\boldsymbol{T}(\psi)\boldsymbol{q}, \tag{3.60}$$

with

$$\boldsymbol{A}_c = \begin{bmatrix} \boldsymbol{0} & \boldsymbol{I} & \boldsymbol{0} \\ \boldsymbol{0} & \boldsymbol{0} & \boldsymbol{I} \\ -\boldsymbol{K}_i & -\boldsymbol{K}_p & -(\boldsymbol{M}^{-1}\boldsymbol{D} + \boldsymbol{K}_d) \end{bmatrix}, \tag{3.61}$$

$$\boldsymbol{T}(\psi) = \begin{bmatrix} \boldsymbol{J}^T(\psi) & \boldsymbol{0} & \boldsymbol{0} \\ \boldsymbol{0} & \boldsymbol{J}^T(\psi) & \boldsymbol{0} \\ \boldsymbol{0} & \boldsymbol{0} & \boldsymbol{I} \end{bmatrix}. \tag{3.62}$$

As the system is controllable, arbitrary eigenvalues can be assigned to matrix $\boldsymbol{A}_c$. Furthermore, because $\boldsymbol{T}^{-1}(\psi) = \boldsymbol{T}^T(\psi)$ for all ψ, the eigenvalues of $\boldsymbol{T}^T(\psi)\boldsymbol{A}_c\boldsymbol{T}(\psi)$ equal those of $\boldsymbol{A}_c$.

In contrast to linear systems, however, $\boldsymbol{A}_c$ being Hurwitz is not a sufficient condition for concluding stability of (3.60). As will become clear in the following, the limiting factor will be the yaw rate $\dot{\psi} = r$. Namely, for small yaw rates, $|r(t)| \leq r_{max}$, asymptotic stability of (3.60) can be concluded and if r_{max} is larger than any physical limit of the system, this stability holds in a global sense. Moreover, increasing the gains in the gain matrices $\boldsymbol{K}_p$, $\boldsymbol{K}_i$ and $\boldsymbol{K}_d$ results in a larger r_{max} due to controllability. This is summarised in the following theorem (see Lindegaard and Fossen, 2003):

Theorem 3.2 (Global Asymptotic Stability of the Controller)
Consider the system (3.51)–(3.52) *with controller* (3.55)–(3.56).
Suppose $|r(t)| \leq r_{max}\ \forall\ t \geq t_0$. *The origin* $\boldsymbol{q} = \boldsymbol{0}$ *of* (3.60) *is locally asymptotically stable, provided* $r_{max} > 0$ *is sufficiently small and if and only if* $\boldsymbol{K}_p$, $\boldsymbol{K}_i$, $\boldsymbol{K}_d$ *are chosen such that* $\boldsymbol{A}_c$ *defined by* (3.61) *is Hurwitz. If* r_{max} *is larger than any physical upper limit for* $|r(t)|$, (3.60) *is said to be globally asymptotically stable.*

Proof. For concluding stability of the closed loop system (3.57)–(3.59), necessity of $\boldsymbol{A}_c$ being Hurwitz is obvious. Sufficiency is proven as follows. First, a transformation $\boldsymbol{z} = \boldsymbol{T}(\psi)\boldsymbol{q}$ is defined. Its time derivative $\dot{\boldsymbol{z}}$ is given by:

$$\dot{\boldsymbol{z}} = \dot{\boldsymbol{T}}(\psi)\boldsymbol{q} + \boldsymbol{T}(\psi)\dot{\boldsymbol{q}} = r\boldsymbol{S}_T\boldsymbol{T}(\psi)\boldsymbol{q} + \boldsymbol{T}(\psi)\boldsymbol{T}^T(\psi)\boldsymbol{A}_c\boldsymbol{T}(\psi)\boldsymbol{q} = (\boldsymbol{A}_c + r\boldsymbol{S}_T)\boldsymbol{z}, \tag{3.63}$$

where the time derivative of $\boldsymbol{T}(\psi)$ is calculated in a similar manner as in equation (2.4):

$$\dot{\boldsymbol{T}}(\psi) = r\boldsymbol{S}_T\boldsymbol{T}(\psi), \text{ with } \quad \boldsymbol{S}_T = \begin{bmatrix} \boldsymbol{S}^T & \boldsymbol{0} & \boldsymbol{0} \\ \boldsymbol{0} & \boldsymbol{S}^T & \boldsymbol{0} \\ \boldsymbol{0} & \boldsymbol{0} & \boldsymbol{0} \end{bmatrix}, \tag{3.64}$$

with $\boldsymbol{S}$ given in (2.4).

If and only if $\boldsymbol{A}_c$ is Hurwitz, there exists a $\boldsymbol{P} = \boldsymbol{P}^T > 0$ such that for a given $\boldsymbol{Q} = \boldsymbol{Q}^T > 0$

$$\boldsymbol{P}\boldsymbol{A}_c + \boldsymbol{A}_c^T\boldsymbol{P} = -\boldsymbol{Q}. \tag{3.65}$$

Next, consider the following positive definite radially unbounded candidate Lyapunov function:

$$V = \boldsymbol{q}^T\boldsymbol{T}^T(\psi)\boldsymbol{P}\boldsymbol{T}(\psi)\boldsymbol{q} = \boldsymbol{z}^T\boldsymbol{P}\boldsymbol{z}. \tag{3.66}$$

Time differentiation and making use of (3.63) yields the following:

$$\begin{aligned}
\dot{V} &= \dot{\boldsymbol{z}}^T \boldsymbol{P}\boldsymbol{z} + \boldsymbol{z}^T \boldsymbol{P}\dot{\boldsymbol{z}} \\
&= \boldsymbol{z}^T(\boldsymbol{P}\boldsymbol{A}_c + \boldsymbol{A}_c^T\boldsymbol{P})\boldsymbol{z} + \boldsymbol{z}^T r(\boldsymbol{P}\boldsymbol{S}_T + \boldsymbol{S}_T^T\boldsymbol{P})\boldsymbol{z} \qquad (3.67) \\
&= -\boldsymbol{z}^T\boldsymbol{Q}\boldsymbol{z} + \boldsymbol{z}^T r(\boldsymbol{P}\boldsymbol{S}_T + \boldsymbol{S}_T^T\boldsymbol{P})\boldsymbol{z} \\
&\leq -\boldsymbol{z}^T\boldsymbol{Q}\boldsymbol{z} + 2|r_{max}|\lambda_{max}(\boldsymbol{P})\|\boldsymbol{z}\|^2 \\
&= -(\lambda_{min}(\boldsymbol{Q}) - 2|r_{max}|\lambda_{max}(\boldsymbol{P}))\|\boldsymbol{q}\|^2. \qquad (3.68)
\end{aligned}$$

Here, λ_{min} and λ_{max} denote the smallest and largest eigenvalue of their respective argument. As can easily be seen from (3.68), $\dot{V}$ is negative definite for r_{max} small enough, which means that (3.60) is asymptotically stable. In fact, this region corresponds to the region of attraction of the closed-loop system. Note that its size only depends on the maximum allowable yaw rate r_{max}. This completes the proof. □

Bound on yaw rate. Moreover, the bound on the yaw rate can be calculated using techniques for linear matrix inequalities, as is shown next. From (3.67), it can be seen that if the function

$$f(r) = \lambda_{max}(\boldsymbol{P}\boldsymbol{A}_c + \boldsymbol{A}_c^T\boldsymbol{P} + r(\boldsymbol{P}\boldsymbol{S}_T + \boldsymbol{S}_T^T\boldsymbol{P})) < 0 \qquad (3.69)$$

for all $t \geq t_0$, then $\dot{V}$ is negative definite and (3.60) is asymptotically stable. As the function $f(r)$ is linear in r, it suffices to show that $f(r_{max}) < 0$ and $f(-r_{max}) < 0$ to conclude that $f(r) < 0$ for all $|r(t)| \leq r_{max}$. For a given closed-loop matrix $\boldsymbol{A}_c$, the bound r_{max} can be calculated by solving a special case of an LMI problem, a so-called generalised eigenvalue problem (see Lindegaard and Fossen, 2003):

$$\begin{aligned}
&\text{minimise } \mu \\
&\text{subject to } \begin{cases} \boldsymbol{P} = \boldsymbol{P}^T > 0, \quad \mu > 0 \\ \boldsymbol{P}\boldsymbol{S}_T + \boldsymbol{S}_T^T\boldsymbol{P} < -\mu(\boldsymbol{P}\boldsymbol{A}_c + \boldsymbol{A}_c^T\boldsymbol{P}) \\ -\boldsymbol{P}\boldsymbol{S}_T - \boldsymbol{S}_T^T\boldsymbol{P} < -\mu(\boldsymbol{P}\boldsymbol{A}_c + \boldsymbol{A}_c^T\boldsymbol{P}) \end{cases}
\end{aligned} \qquad (3.70)$$

where $r_{max} = 1/\mu$. This generalised eigenvalue problem can be efficiently solved using for instance the LMI-toolbox in MATLAB (Gahinet et al., 1995).

3.4 Dynamic Positioning System

Now that the observer and the controller have been derived separately in the previous two sections, they have to be combined to obtain the complete dynamic positioning system.

Therefore, new error variables are defined similar to (3.54), in which the state estimates from the observer are used:

$$\hat{\boldsymbol{\eta}}_e = \hat{\boldsymbol{\eta}} - \boldsymbol{\eta}_d, \qquad \hat{\boldsymbol{\nu}}_e = \hat{\boldsymbol{\nu}} - \boldsymbol{\nu}_d. \tag{3.71}$$

Next, the control law (3.55)–(3.56) is modified to contain these new error variables. Moreover, the estimated heading angle $\hat{\psi}$ is used instead of ψ. The following observer-feedback controller results:

$$\dot{\boldsymbol{\xi}} = \hat{\boldsymbol{\eta}}_e, \tag{3.72}$$

$$\hat{\boldsymbol{\tau}} = -\boldsymbol{M}(\boldsymbol{K}_i \boldsymbol{J}^T(\hat{\psi})\boldsymbol{\xi} + \boldsymbol{K}_p \boldsymbol{J}^T(\hat{\psi})\hat{\boldsymbol{\eta}}_e + \boldsymbol{K}_d \hat{\boldsymbol{\nu}}_e) + \boldsymbol{D}\boldsymbol{\nu}_d + \boldsymbol{M}\dot{\boldsymbol{\nu}}_d. \tag{3.73}$$

Because of the estimated heading angle, the state estimates appear non-affinely in the control $\hat{\boldsymbol{\tau}}$. However, due to the inherently linear characteristics of the system and the linear bound in $\|\boldsymbol{J}(\hat{\psi}) - \boldsymbol{I}\|$, asymptotic stability can still be concluded. This is summarised in the following theorem:

Theorem 3.3 (Global Asymptotic Stability of the Total System)
For the system (3.51)–(3.52) *there exists an observer whose errors* $\tilde{\boldsymbol{\eta}}$ *and* $\tilde{\boldsymbol{\nu}}$ *converge asymptotically to zero (see Theorem 3.1). The observer-feedback control* (3.72)–(3.73) *will, then, guarantee global asymptotical stability of* $\boldsymbol{q} = [\boldsymbol{\xi}^T, \boldsymbol{\eta}_e^T, \boldsymbol{\nu}_e^T]^T$ *under the same assumptions as stated in Theorem 3.2, namely:*

1. *The gains* $\boldsymbol{K}_p$, $\boldsymbol{K}_i$ *and* $\boldsymbol{K}_i$ *are chosen such that* $\boldsymbol{A}_c$, *defined in* (3.61) *is Hurwitz,*
2. *The yaw-rate is smaller than the upper bound following from the stability analysis of the controller, that is* $|r(t)| \leq r_{max}$.

Proof. In equations (3.72)–(3.73), the observer-feedback controller was given. By definition, in the derivation of the observer it is given that $\hat{\boldsymbol{\eta}} = \boldsymbol{\eta} - \tilde{\boldsymbol{\eta}}$ and $\hat{\boldsymbol{\nu}} = \boldsymbol{\nu} - \tilde{\boldsymbol{\nu}}$, which yields the following expressions for the error terms:

$$\hat{\boldsymbol{\eta}}_e = \hat{\boldsymbol{\eta}} - \boldsymbol{\eta}_d = \boldsymbol{\eta} - \boldsymbol{\eta}_d - \tilde{\boldsymbol{\eta}} = \boldsymbol{\eta}_e - \tilde{\boldsymbol{\eta}}, \tag{3.74}$$

$$\hat{\boldsymbol{\nu}}_e = \hat{\boldsymbol{\nu}} - \boldsymbol{\nu}_d = \boldsymbol{\nu} - \boldsymbol{\nu}_d - \tilde{\boldsymbol{\nu}} = \boldsymbol{\nu}_e - \tilde{\boldsymbol{\nu}}. \tag{3.75}$$

Furthermore, the term with the rotation matrix can be rewritten as:

$$\boldsymbol{J}^T(\hat{\psi}) = \boldsymbol{J}^T(\psi - \tilde{\psi}) = \boldsymbol{J}^T(\psi) + \boldsymbol{J}^T(\psi)(\boldsymbol{J}(\tilde{\psi}) - \boldsymbol{I}). \tag{3.76}$$

To save space, the rotation matrix will, in the following, be denoted with a subscript

notation: $\boldsymbol{J}_a \equiv \boldsymbol{J}(a)$. Applying (3.74)–(3.76) to the input (3.73) gives:

$$\begin{aligned}
\hat{\boldsymbol{\tau}} &= -\boldsymbol{M}\left(\boldsymbol{K}_i[\boldsymbol{J}_\psi^T + \boldsymbol{J}_\psi^T(\boldsymbol{J}_{\tilde{\psi}} - \boldsymbol{I})]\boldsymbol{\xi} + \boldsymbol{K}_p[\boldsymbol{J}_\psi^T + \boldsymbol{J}_\psi^T(\boldsymbol{J}_{\tilde{\psi}} - \boldsymbol{I})](\boldsymbol{\eta}_e - \tilde{\boldsymbol{\eta}}) + \boldsymbol{K}_d(\boldsymbol{\nu}_e - \tilde{\boldsymbol{\nu}})\right) \\
&\quad + \boldsymbol{D}\boldsymbol{\nu}_d + \boldsymbol{M}\dot{\boldsymbol{\nu}}_d \\
&= -\boldsymbol{M}\left(\boldsymbol{K}_i\boldsymbol{J}_\psi^T\boldsymbol{\xi} + \boldsymbol{K}_p\boldsymbol{J}_\psi^T\boldsymbol{\eta}_e + \boldsymbol{K}_d\boldsymbol{\nu}_e\right) + \boldsymbol{D}\boldsymbol{\nu}_d + \boldsymbol{M}\dot{\boldsymbol{\nu}}_d \\
&\quad -\boldsymbol{M}\left(\boldsymbol{K}_i[\boldsymbol{J}_\psi^T(\boldsymbol{J}_{\tilde{\psi}} - \boldsymbol{I})]\boldsymbol{\xi} + \boldsymbol{K}_p[\boldsymbol{J}_\psi^T(\boldsymbol{J}_{\tilde{\psi}} - \boldsymbol{I})]\boldsymbol{\eta}_e - \boldsymbol{K}_p\boldsymbol{J}_\psi^T\boldsymbol{J}_{\tilde{\psi}}\tilde{\boldsymbol{\eta}} - \boldsymbol{K}_d\tilde{\boldsymbol{\nu}}\right) \\
&= \boldsymbol{\tau} - \boldsymbol{M}\left(\boldsymbol{K}_i[\boldsymbol{J}_\psi^T(\boldsymbol{J}_{\tilde{\psi}} - \boldsymbol{I})]\boldsymbol{\xi} + \boldsymbol{K}_p[\boldsymbol{J}_\psi^T(\boldsymbol{J}_{\tilde{\psi}} - \boldsymbol{I})]\boldsymbol{\eta}_e - \boldsymbol{K}_p\boldsymbol{J}_\psi^T\boldsymbol{J}_{\tilde{\psi}}\tilde{\boldsymbol{\eta}} - \boldsymbol{K}_d\tilde{\boldsymbol{\nu}}\right), \qquad (3.77)
\end{aligned}$$

where $\boldsymbol{\tau}$ equals the original control (see equation (3.56)). Consequently, the following closed loop system is obtained:

$$\begin{aligned}
\dot{\boldsymbol{\xi}} &= \boldsymbol{\eta}_e - \tilde{\boldsymbol{\eta}}, && (3.78)\\
\dot{\boldsymbol{\eta}}_e &= \boldsymbol{J}_\psi\boldsymbol{\nu}_e, && (3.79)\\
\dot{\boldsymbol{\nu}}_e &= -(\boldsymbol{M}^{-1}\boldsymbol{D} + \boldsymbol{K}_d)\boldsymbol{\nu}_e - \boldsymbol{K}_p\boldsymbol{J}_\psi^T\boldsymbol{\eta}_e - \boldsymbol{K}_i\boldsymbol{J}_\psi^T\boldsymbol{\xi} \\
&\quad -\boldsymbol{K}_i[\boldsymbol{J}_\psi^T(\boldsymbol{J}_{\tilde{\psi}} - \boldsymbol{I})]\boldsymbol{\xi} - \boldsymbol{K}_p[\boldsymbol{J}_\psi^T(\boldsymbol{J}_{\tilde{\psi}} - \boldsymbol{I})]\boldsymbol{\eta}_e + \boldsymbol{K}_p\boldsymbol{J}_\psi^T\boldsymbol{J}_{\tilde{\psi}}\tilde{\boldsymbol{\eta}} + \boldsymbol{K}_d\tilde{\boldsymbol{\nu}}. && (3.80)
\end{aligned}$$

The estimation errors $\tilde{\boldsymbol{\eta}}$ and $\tilde{\boldsymbol{\nu}}$ can, in this way, be seen as perturbation terms, connecting the observer error dynamics to the closed loop dynamics. Using $\boldsymbol{q} = [\boldsymbol{\xi}^T, \boldsymbol{\eta}_e^T, \boldsymbol{\nu}_e^T]^T$ and $\tilde{\boldsymbol{q}} = [\tilde{\boldsymbol{\eta}}^T, \tilde{\boldsymbol{\nu}}^T]^T$, (3.78)–(3.80) are written in state-space form:

$$\dot{\boldsymbol{q}} = \boldsymbol{T}^T(\psi)\boldsymbol{A}_c\boldsymbol{T}(\psi)\boldsymbol{q} + \boldsymbol{g}(\boldsymbol{q}, \tilde{\boldsymbol{q}}), \qquad (3.81)$$

where $\boldsymbol{A}_c$ and $\boldsymbol{T}(\psi)$ are defined in (3.61) and (3.62), respectively. The perturbation term $\boldsymbol{g}(\boldsymbol{q}, \tilde{\boldsymbol{q}})$ has the following structure:

$$\boldsymbol{g}(\boldsymbol{q}, \tilde{\boldsymbol{q}}) = \begin{bmatrix} \boldsymbol{g}_1 \\ \boldsymbol{0} \\ \boldsymbol{g}_3 \end{bmatrix}, \qquad (3.82)$$

with the individual terms:

$$\begin{aligned}
\boldsymbol{g}_1 &= -\tilde{\boldsymbol{\eta}}, && (3.83)\\
\boldsymbol{g}_3 &= -\boldsymbol{K}_i[\boldsymbol{J}_\psi^T(\boldsymbol{J}_{\tilde{\psi}} - \boldsymbol{I})]\boldsymbol{\xi} - \boldsymbol{K}_p[\boldsymbol{J}_\psi^T(\boldsymbol{J}_{\tilde{\psi}} - \boldsymbol{I})]\boldsymbol{\eta}_e + \boldsymbol{K}_p\boldsymbol{J}_\psi^T\boldsymbol{J}_{\tilde{\psi}}\tilde{\boldsymbol{\eta}} + \boldsymbol{K}_d\tilde{\boldsymbol{\nu}}. && (3.84)
\end{aligned}$$

This output-feedback system can be regarded as a cascaded system, containing the error dynamics of both the state feedback system and the observer:

$$\begin{aligned}
\Sigma_1: \quad \dot{\boldsymbol{q}} &= \boldsymbol{T}^T(\psi)\boldsymbol{A}_c\boldsymbol{T}(\psi)\boldsymbol{q} + \boldsymbol{g}(t, \boldsymbol{q}, \tilde{\boldsymbol{q}}), && (3.85)\\
\Sigma_2: \quad \dot{\tilde{\boldsymbol{q}}} &= \boldsymbol{f}_{\tilde{\boldsymbol{q}}}(t, \tilde{\boldsymbol{q}}), && (3.86)
\end{aligned}$$

where system Σ_2 contains the relevant observer error dynamics. Furthermore, the observer error dynamics have been shown to be globally asymptotically stable in Theorem 3.1.

Additionally, Theorem 3.2 assures stability of Σ_1 with $\boldsymbol{g}(t, \boldsymbol{q}, \tilde{\boldsymbol{q}}) = \boldsymbol{0}$ for bounded yaw rates (the limit r_{max}). Thus, the stable system Σ_1 is perturbed with the asymptotically decaying observation error. For concluding stability of this cascaded system, results from Panteley and Loria (1998) are used. However, a slightly modified version of these results is given in Lindegaard (2003), which states that the cascaded system is stable if:

- the unperturbed system Σ_1 is globally asymptotically stable and satisfies some bounds on a Lyapunov function (these bounds are not explained here);
- the function $\boldsymbol{g}(t, \boldsymbol{q}, \tilde{\boldsymbol{q}})$ satisfies the following bound:

$$\|\boldsymbol{g}(t, \boldsymbol{q}, \tilde{\boldsymbol{q}})\| \leq \theta_1(\|\tilde{\boldsymbol{q}}\|) + \theta_2(\|\tilde{\boldsymbol{q}}\|)\|\boldsymbol{q}\|, \tag{3.87}$$

  where $\theta_i : \mathbb{R}_{\geq 0} \rightarrow \mathbb{R}_{\geq 0}$ for $i = 1, 2$ are continuous and $\theta_i(0) = 0$.

The first condition is satisfied from Theorem 3.2. For details, see Lindegaard (2003). This means that for concluding stability of the total system (3.85)–(3.86) , it has to be checked whether the function $\boldsymbol{g}(t, \boldsymbol{q}, \tilde{\boldsymbol{q}})$ satisfies the bound in the second condition. This is done in equation (3.88), where use is made of the fact that $\|\boldsymbol{J}^T(\psi)\| = 1$ and $\|\boldsymbol{J}(\tilde{\psi}) - \boldsymbol{I}\| \leq 2|\tilde{\psi}|$.

$$\begin{aligned} \|\boldsymbol{g}\| &\leq \|\tilde{\boldsymbol{\eta}}\| + 2\|\boldsymbol{K}_i\||\tilde{\psi}|\|\boldsymbol{\xi}\| + 2\|\boldsymbol{K}_p\||\tilde{\psi}|\|\boldsymbol{\eta}_e\| + \|\boldsymbol{K}_p\|\|\tilde{\boldsymbol{\eta}}\| + \|\boldsymbol{K}_d\|\|\tilde{\boldsymbol{\nu}}\| \\ &= \theta_1(\|\boldsymbol{q}\|) + \theta_2(\|\tilde{\boldsymbol{q}}\|)\|\boldsymbol{q}\|, \end{aligned} \tag{3.88}$$

with the following linear functions $\theta_i : \mathbb{R}_{\geq 0} \rightarrow \mathbb{R}_{\geq 0}$ for $i = 1, 2$:

$$\theta_1(\|\tilde{\boldsymbol{q}}\|) = (1 + \|\boldsymbol{K}_p\| + \|\boldsymbol{K}_d\|)\|\tilde{\boldsymbol{q}}\|, \tag{3.89}$$

$$\theta_2(\|\tilde{\boldsymbol{q}}\|) = 2(\|\boldsymbol{K}_i\| + \|\boldsymbol{K}_p\|)|\tilde{\psi}|. \tag{3.90}$$

As these functions satisfy the requirements stated in the second condition above, the proof is complete, meaning that the cascaded system is globally asymptotically stable. □

Chapter 4

Experimental Setup

In this chapter, a description of the experimental setup for the dynamic positioning system is given. Next, some features of this setup are discussed more in detail in section 4.2 and 4.3. Furthermore, a spectrum of the wave-induced motion of the ship is given and the model parameter identification is described in sections 4.4 and 4.5, respectively.

4.1 Setup Description

In figure 4.1, a schematic representation of the experimental setup can be seen.

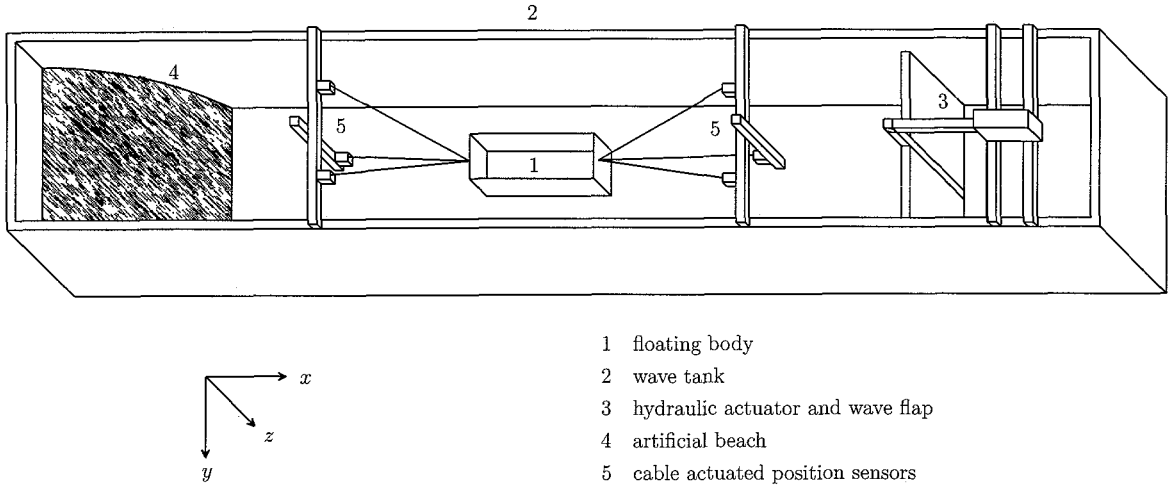

Figure 4.1: Schematic representation of the experimental setup.

In this setup, the floating body is located in a wave tank (15 m×1.5 m×1.5 m), in which waves can be generated by means of a wave flap at one end of the tank. This wave flap

is operated by a hydraulic actuator moving in harmonic motion. Both the amplitude and the frequency of this motion can be prescribed, corresponding to the resulting wave height and frequency, respectively. At the other end of the wave tank, an artificial beach prevents wave reflection.

As can also be seen in figure 4.1, six thin wires (⌀ 0.45 mm) are connected to the floating body. These wires consist of a part with fixed length and a part that comes from a cable actuated position sensor (the WS10SG from ASM Automation Sensorik Messtechnik GmbH). This electromechanical sensor translates linear motion into a proportional electrical signal. The cable, with a length of 1 m, winds onto a cable drum on a shaft, which is tensioned by a coil spring, providing a specified constant pull-in force (approximately 3 N) to maintain cable tension. This rotary motion is converted to an electrical signal by means of a precision potentiometer. In section 4.2, the position measurement of the floating body will be discussed in detail.

The dynamic positioning system, as discussed in chapter 3 is implemented on a 2.5 GHz Pentium PC with 2 GB RAM. This PC collects the data from the position sensors via a measurement card (from Meilhaus Electronic) and sends data to the propulsion devices through the serial port. The DP system is designed using MATLAB/SIMULINK. Using the Real Time Workshop in MATLAB and the Simulation Interface Toolkit from LabVIEW, the model is compiled in order to be able to use the model in LabVIEW. Here, the connection between the computer and the input/output ports is established such that the dynamic positioning system can be tested on the experimental setup.

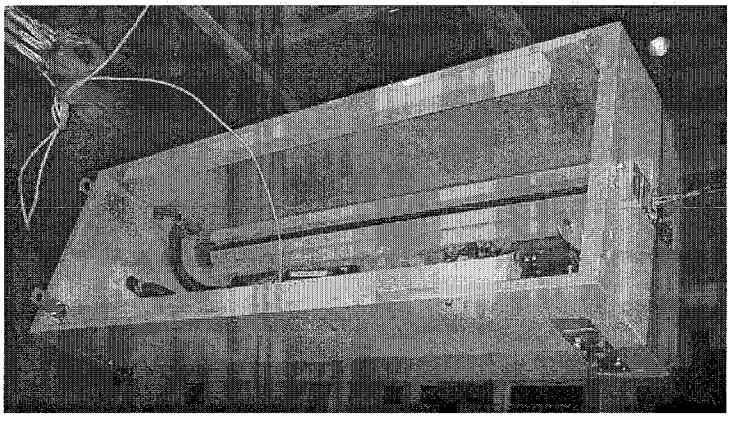

Figure 4.2: Picture of the floating body in the wave tank.

A picture of the floating body can be seen in figure 4.2. The wooden body has a length of 1.37 m, a width of 0.46 m and a height of 0.41 m. Furthermore, the two edges in length direction at the bottom side are chamfered. In order to obtain a draught of approximately 0.20 m, weight is added in the form of steel rods. Because the floating body is to be kept

at velocities around zero, rudders can not be used in the positioning system. Instead, as a propulsion system, thrusters are used, which can operate only one way. These thrusters pump water from below the body through tubes to the thruster outputs located in the sides of the body. In total, six thrusters are located in the body such that the three degrees of freedom of interest can be controlled. Each thruster is driven by a brushless DC electromotor, controlled by a separate unit that maintains the desired rotational velocity. The separate thruster units are powered by two battery packs of 9.6 V each. The rotational velocity results from an input signal to the control unit which is a hexadecimal number between 00 and FF (between 0 and 255 in decimal notation). On a printed circuit board, a programmable microcontroller is located for each control unit, in whose memory a table is stored that contains the relation between the given input number and the actual input number. Thus, the relation between the input and the rotational velocity can be prescribed/modified.

Moreover, for the controller, it is important to determine how the thruster outputs are located in the body. This is depicted in figure 4.3.

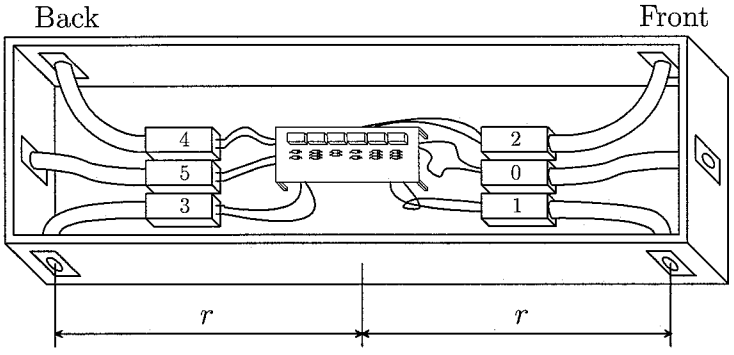

Figure 4.3: Drawing of the body, with the location of thrusters 0 to 5.

The relation between the control $\boldsymbol{\tau}$ and the thruster outputs can be described by the so-called thruster configuration matrix $\boldsymbol{B}_\tau$ and is given in the following relation:

$$\boldsymbol{\tau} = \boldsymbol{B}_\tau \boldsymbol{u}, \tag{4.1}$$

where the input vector $\boldsymbol{u} = [f_0, f_1, f_2, f_3, f_4, f_5]^T$ contains the thruster forces. The thruster configuration matrix equals:

$$\boldsymbol{B}_\tau = \begin{bmatrix} -1 & 0 & 0 & 0 & 0 & 1 \\ 0 & -1 & 1 & -1 & 1 & 0 \\ 0 & -r & r & r & -r & 0 \end{bmatrix}. \tag{4.2}$$

The variable r denotes the horizontal distance from the thruster output to the center of gravity of the body as seen in figure 4.3. More information on the thrusters follows in section 4.3, together with the procedure to modify the input-output behaviour.

In the next four sections, various parts of the experimental setup are discussed more in detail, in order to be able to use the dynamic positioning system in practice.

4.2 Position Measurement

In order to uniquely determine the position of the floating body, cable actuated position sensors are used as, due to the limited time for the project, contactless measurements were impossible. Three cables (from sensors 1, 2 and 3) are attached to a point at the front of the ship and three (sensors 4, 5 and 6) to a point at the back. In this way, all ship positions and orientation angles can be determined except the roll angle ϕ about an axis through these two points. For the dynamic positioning system, however, only x, y and ψ are necessary. The sensor positions can be described by vectors $\boldsymbol{x}_i = [x_i, y_i, z_i]^T$ $(i = 1, \ldots, 6)$, relative to an origin located at a fixed point in the wave tank. These positions have been measured and are given in table 4.1.

Table 4.1: Sensor position coordinates.

Sensor	x_i [m]	y_i [m]	z_i [m]
1	2.828	0.511	0.206
2	2.908	0.799	0.526
3	2.828	1.103	0.206
4	10.752	0.505	0.206
5	10.578	0.805	0.525
6	10.752	1.100	0.206

The position vectors of the points at the front and the back of the floating body are obtained from calculations, given in appendix B. In this way, the vectors

$$\boldsymbol{x}_f = [x_f, y_f, z_f]^T \quad \text{and} \quad \boldsymbol{x}_b = [x_b, y_b, z_b]^T \tag{4.3}$$

are computed. Next, the horizontal positions and the heading angle of the ship follow from

$$x = -\frac{x_f + x_b}{2} + x_{ref}, \tag{4.4}$$

$$y = \frac{y_f + y_b}{2} - y_{ref}, \tag{4.5}$$

$$\psi = \arctan\left(\frac{y_f - y_b}{x_b - x_f}\right) - \psi_{ref}, \tag{4.6}$$

where x_{ref} and y_{ref} are the rest positions of the floating body. For the heading angle, a very small compensation ψ_{ref} is necessary, due to inaccuracy in the measured sensor positions. Due to measurement noise from the cable actuated position sensors, the calculated position will also contain noise. The standard deviations of this noise is determined experimentally and given in table 4.2, together with the reference positions/angle. Furthermore, due to the relative small angle between the three cables at one side of the body, the resolution of the position measurement is not the same for the three directions. The sensors themselves have a resolution of approximately 1 mm. An experimentally determined estimate of the resolution in the separate directions is also given in table 4.2.

Table 4.2: Measurement reference positions/angle and standard deviation of the measurement noise.

Coordinate	Reference [m] or [rad]	σ_i [m] or [rad]	Resolution [m] or [rad]
x	6.899	$9.5{\cdot}10^{-5}$	$1{\cdot}10^{-3}$
y	0.840	$5.5{\cdot}10^{-4}$	$5{\cdot}10^{-3}$
ψ	0.006	$7.6{\cdot}10^{-4}$	$1{\cdot}10^{-2}$

4.3 Thruster Curves

As already described in section 4.1, a programmable microcontroller is available for each thruster, which stores the relation between the given input number and the actual input number (both between 0 and 255). This can be used to modify the input-force curves of the thrusters and to obtain a linear relation between the input number and the force. In order to do this, the thruster force has to be measured.

For this purpose, a thin steel wire is tied to the floating body at a thruster output. This wire guides the thruster force, by means of a pulley, to a force transducer, whose working principle is based on strain gauges. As a result, a voltage, proportional to the thruster force is obtained. For a large number of input values, the corresponding thruster forces are measured for each thruster in this way. During operation, the motors warm up, which has influence on the thruster characteristics. Furthermore, the thrusters show different behaviour for increasing and decreasing input values.

Next, these curves are modified, using the look-up table in the microcontroller memory,

such that a linear relation between the input number and the thruster force is obtained. In this approach, the values for the increasing and decreasing input values are averaged. After that, the curves are measured again. This can be seen in figure 4.4, where, additionally, a linear fit to the modified curve is made using least squares. This fit will be used in the dynamic positioning controller.

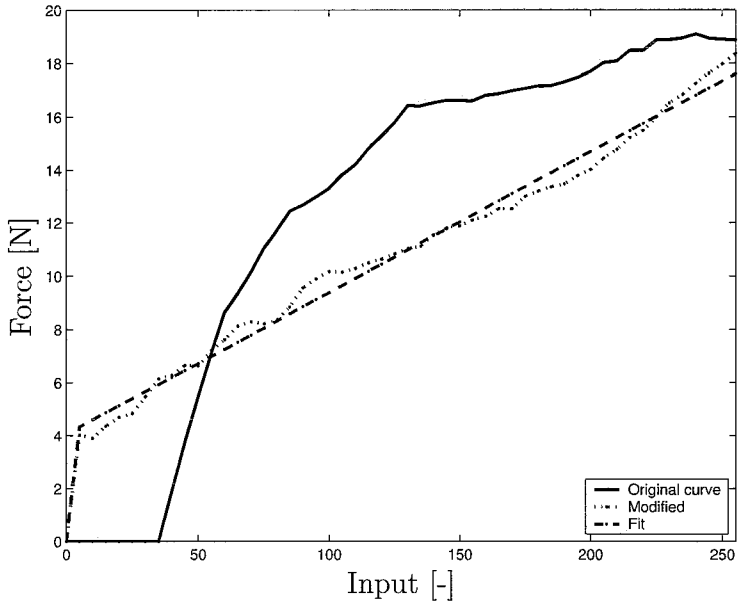

Figure 4.4: Example of an original, modified and fitted thruster curve for thruster 1.

In this figure, it can be seen that the behaviour of the modified curve is approximately linear. A problem, however, is that for small input numbers, already a relative large force is generated by the thruster. This comes from the fact that the thruster device needs a certain minimum force to generate a water flow due to pressure losses. As this behaviour is inherent to the thruster devices, it will be included in the controller. Hence, the relation between the input n and the thruster force f_i $(i = 0, \ldots, 5)$ is given by:

$$f_i = \begin{cases} 0 & \text{for } n = 0 \\ f_{0i} + f_{1i} n & \text{for } n > 0 \end{cases} \quad \text{for } i = 0, \ldots, 5, \tag{4.7}$$

where the constant and linear terms for each thruster are given in table 4.3.

Obviously, thruster 0 has a different characteristic. This is caused by the fact that the thruster unit showed increased wear due to an alignment mismatch between the motor and the pump part. After modification of the curve, however, this results in a lower minimum force. Furthermore, the thrusters do not have the same threshold value in force (the second column in table 4.3), which causes difficulties for the dynamic positioning system in the experimental setup as will become clear in chapter 5.

Table 4.3: Thruster curve parameters for the linear fit.

Thruster	f_{0i} [N]	f_{1i} [N/-]
0	0.60	0.068
1	4.08	0.053
2	3.24	0.056
3	3.35	0.060
4	2.74	0.059
5	2.86	0.055

4.4 Wave-Induced Motion

In the previous chapter, it is explained that a wave model will be used in the observer design. Therefore, the wave-induced motion of the floating body is measured for some settings of the hydraulic actuator of the wave flap (amplitude and frequency), such that it can be determined whether the wave and drift models provide proper approximations. For this purpose, the position of the ship is measured for five minutes. Next, spectral analysis of this signal is carried out in MATLAB. An example of the amplitude plots of the spectra for the three degrees of freedom is given in figure 4.5.

Note, that the high frequent measurement noise can be seen in the spectra, as well as the low-frequent second order wave drift. It can also be seen that, especially in y and ψ-direction, low frequencies are present in the measured signal. This is caused by a slow combined swaying and yawing movement, due to the influence of the cable actuated position sensors. This low-frequent periodic motion cannot be described properly by the drift model. However, this causes no problems, as will be seen in chapter 5.

Furthermore, figure 4.5 shows the wave-induced motions, approximated using the fourth order wave model, described in section 2.2.1, after some manual model parameter tuning. It can be seen that a good match is obtained for the dominant wave frequency, which means that the fourth-order wave model is suitable to describe the wave-induced motion. The parameters for this situation are given in table 4.4.

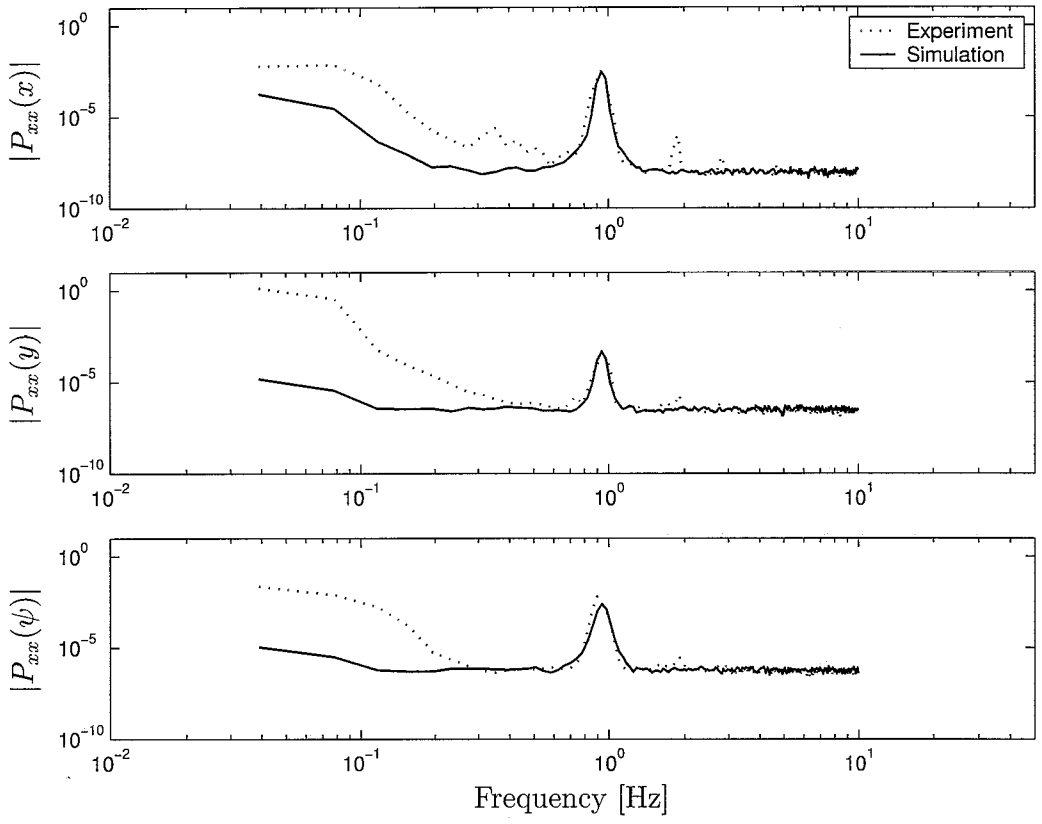

Figure 4.5: Example of the wave-induced motion for a wave frequency of $f = 0.94$ Hz and a wave flap voltage of $V = 200$ mV.

Table 4.4: Example of the parameter values for the wave model (values correspond to the spectra in figure 4.5). k_{wi} and k_{bi} are the noise intensities in the first and second order wave disturbance models, respectively.

Direction	ω_{0i} [rad/s]	ξ_i [-]	k_{wi}	k_{bi}
x	1.88π	0.01	0.01	0.02
y	1.88π	0.02	0.01	0.02
ψ	1.88π	0.03	0.05	0.002

4.5 Parameter Identification

In order to use the dynamic positioning system, designed in chapter 3, the parameters in the model have to be identified. Parameters like m and I_z are measured using a mass balance and a special setup for measuring the moment of inertia, respectively. Furthermore, the body-fixed coordinate system is chosen to coincide with the centre of gravity and the

dimensions of the model are measured.

In order to obtain expressions for the added mass and potential damping of the system, the numerical software package AQWA is used. Using the finite element program FemGV, a mesh of the body surface is created. Next, using radiation/diffraction theory, the added mass and potential damping are calculated for a range of frequencies in AQWA. In order to find the appropriate added mass and damping values for dynamic positioning, the obtained curves are evaluated for zero frequency ($\lim_{f\to 0} \boldsymbol{M}_A$). These curves, however, are only estimates, because added mass is highly influenced by the presence of walls and finite water depth, as is the case in the experiment.

The potential damping evaluates to be zero for low frequencies, as stated in appendix A.3.2. Furthermore, other damping terms contribute to the damping matrix $\boldsymbol{D}$. As it is very difficult to obtain or measure these parameters in a straightforward manner, values from Strand (1999) are used after applying some scaling. Namely, the parameters for a model ship, smaller than the floating body in this project, are given here. As a consequence, some robustness analysis of the dynamic positioning system has to be performed for these damping parameters.

Summarising, this results in the model parameters given in table 4.5.

Table 4.5: Parameter values.

Parameter	Value		Parameter	Value	
m	127.9	kg	$N_{\dot{r}}$	-11.4	kg m^2
I_z	19.8	kg m^2	X_u	-20.0	N s/m
x_G	0.0	m	Y_v	-70.0	N s/m
$X_{\dot{u}}$	-29.5	kg	Y_r	0.0	N s
$Y_{\dot{v}}$	-110.0	kg	N_v	0.0	N s
$Y_{\dot{r}}$	0.0	kg m	N_r	-10.0	N m s
$N_{\dot{v}}$	0.0	kg m	r	0.605	m

Chapter 5

Simulations and Experiments

In this chapter, the simulation and experimental results for the dynamic positioning system will be discussed for a typical experiment. First, however, some implementation issues are discussed in section 5.1.

5.1 Implementation Issues

As stated in section 4.1, the dynamic positioning system is designed in MATLAB/SIMULINK. Moreover, the combination between the desired input (3.73) and the thruster forces, using the thruster configuration matrix $\boldsymbol{B}_{\boldsymbol{\tau}}$ in (4.2), is established. Namely, for each thruster, a lookup table is included with the thruster curve (as found in section 4.3). In order to take into account the threshold values in these curves, an overall threshold values for the thrusters, used for sway and yaw direction of the body, is implemented. This threshold value equals the largest threshold value in table 4.3. Due to the differences in threshold values, this would otherwise lead to differences in the forces between two thrusters that are to apply an equal force. In this way, thrusters 1, 2, 3 and 4 cannot generate a force below 4.08 N. This affects the performance of the dynamic positioning system in a disadvantageous way, but no other solution was found for this.

Furthermore, the algorithm for the position measurement (see appendix B) is implemented in SIMULINK. After the model is compiled and combined with LabVIEW, it has the six wire lengths as input from the experimental setup and gives six thruster input values as output to the thruster devices.

Finally, in both the simulations and the experiments, a fixed step solver is used. After some initial experimenting, the ODE4-solver (fourth-order Runge-Kutta) is found to give satisfactory results.

5.2 Simulation Results

In this section, the simulation results will be discussed for a wave frequency of $f = 0.94$ Hz and a wave flap voltage amplitude of $V = 200$ mV. This experiment will also be used in the next section and is considered to be representative for the movements that the floating body can undergo. A part of the measured position, used for calculating the spectra in figure 4.5, is depicted in figure 5.1.

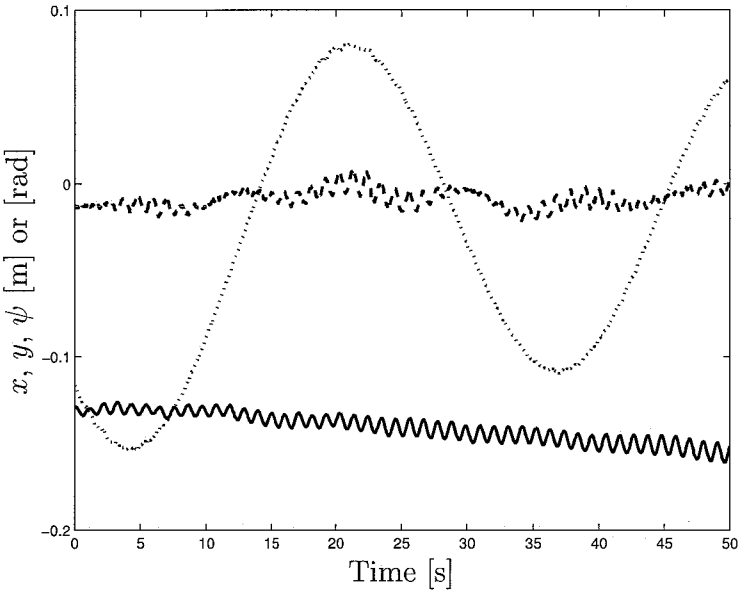

Figure 5.1: Part of the measured position: x (solid), y (dotted), ψ (dashed).

The spectrum of the wave induced motion at this particular setup is depicted in figure 4.5 and the wave and drift model parameters are given in table 4.4.

5.2.1 Observer Tuning

Firstly, the observer has to be designed to be strictly positive real (SPR), by choosing the observer gains k_{ji}, $j = 1, \ldots, 7$, $i = 1, 2, 3$ according to equations (3.41)–(3.46). Using these equations, a relatively straightforward tuning procedure can be used, as, for each degree of freedom, only five parameters have to be tuned (ω_{0i}, ξ_{ni}, ω_{ci}, k_{6i}, k_{7i}, $i = 1, 2, 3$). Additionally, the parameter γ has to be chosen. After some tuning, the parameters, given in table 5.1 are found.

An example of the typical form of the transfer function was already given in figure 3.3 for yaw-direction. The notch effect and the low pass-filter can clearly be seen here, as well as the high low-frequent gain, enabling proper second-order wave drift estimates. The

Table 5.1: Observer parameters to satisfy the SPR requirement. Additionally, $\gamma = 0.1$.

Direction	ω_{0i} [rad/s]	ξ_{ni} [-]	ω_{ci} [rad/s]	k_{6i}	k_{7i}
x	1.88π	0.03	3.2π	20	200
y	1.88π	0.06	3.2π	20	200
ψ	1.88π	0.09	3.2π	5	50

parameters in the last two columns in table 5.1 are found from simulations in the time domain.

An example of the behaviour of the observer can be seen in figure 5.2, where the results of a simulation using only the observer are depicted. In this figure, both the measured (simulated) and estimated position are depicted.

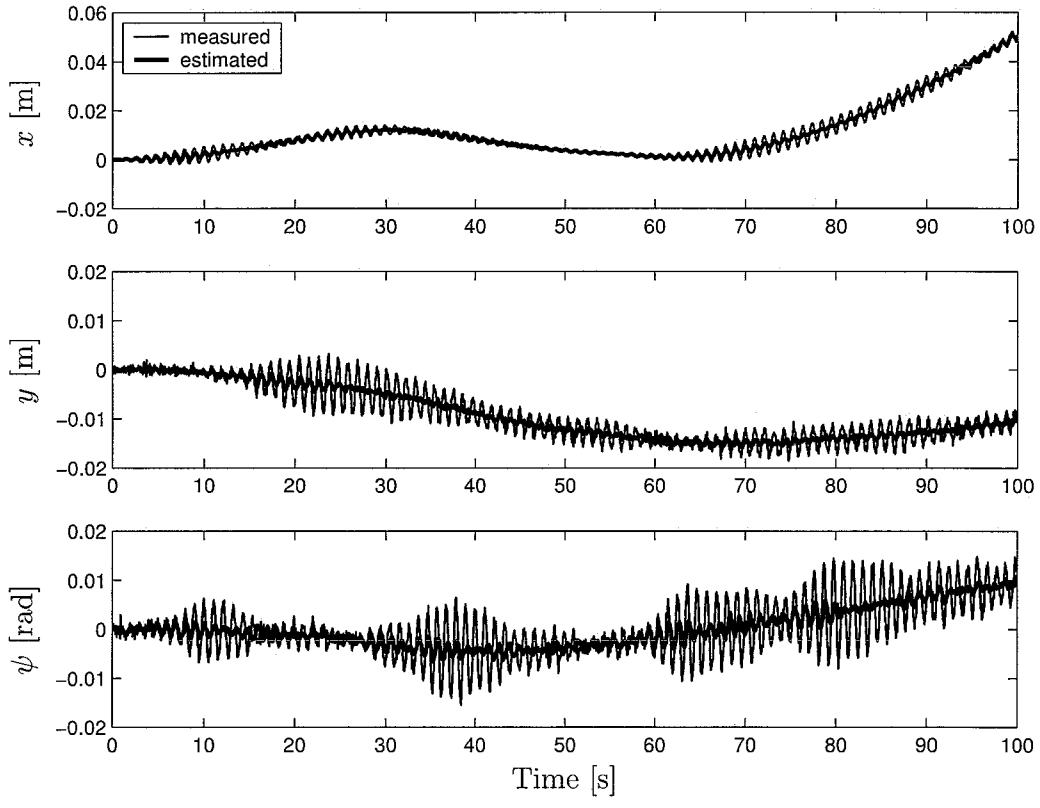

Figure 5.2: Simulation of the measured (thin line) and estimated (thick line) position using the observer.

From this figure, it becomes clear that the observer succeeds in filtering a large portion of the first order wave disturbances from the measured signal. however, because of the

SPR-requirement, there is limited tuning freedom in the observer. As a result, the notch in the observer transfer function cannot be arbitrary deep and the filtering of the first order wave disturbances is not complete.

5.2.2 Controller Tuning

Next, the controller has to be tuned. This can, for instance, be done by pole placement or by loop shaping techniques. In the latter, it should be noted that *only* a PID-controller can be used. However, a notch filter and a low-pass filter are already included in the observer.

In the case, discussed here, loop shaping techniques are used, where the cross-over frequency is set to approximately 0.2 Hz. As both the mass matrix and the damping matrix are diagonal, the total system can be seen as three decoupled SISO systems, resulting in diagonal gain matrices. After some tuning, the values in table 5.2 are found for the elements in the proportional, derivative and integrating gain matrices ($\boldsymbol{K}_p$, $\boldsymbol{K}_d$ and $\boldsymbol{K}_i$, respectively). Note, that for all three directions, the same controller is used.

Table 5.2: Parameter values for the PID-controller.

Direction	k_p	k_d	k_i
x	8.0	6.37	0.50
y	8.0	6.37	0.50
ψ	8.0	6.37	0.50

Furthermore, the maximum allowable yaw rate for concluding stability for this controller is calculated using LMI techniques, as described in section 3.3.3. This results in $r_{max} = 28.7$ rad/s, which is assumed to be larger than the maximum achievable yaw rate of the system. Hence, this controller is stable in a global sense.

Simulation results with this controller are depicted in figure 5.3, where the dynamic positioning system (both the observer and controller) is switched on after 60 seconds. In this figure, it can be seen that the DP system succeeds in bringing the floating body back to the origin. However, asymptotic stability is not achieved. This is caused by both the incomplete wave-filtering, as stated in the previous section, and the threshold values of the thrusters. Namely, the thrusters cannot produce the necessary small forces to reduce small position errors. In spite of these shortcomings, however, the resulting positioning error is small.

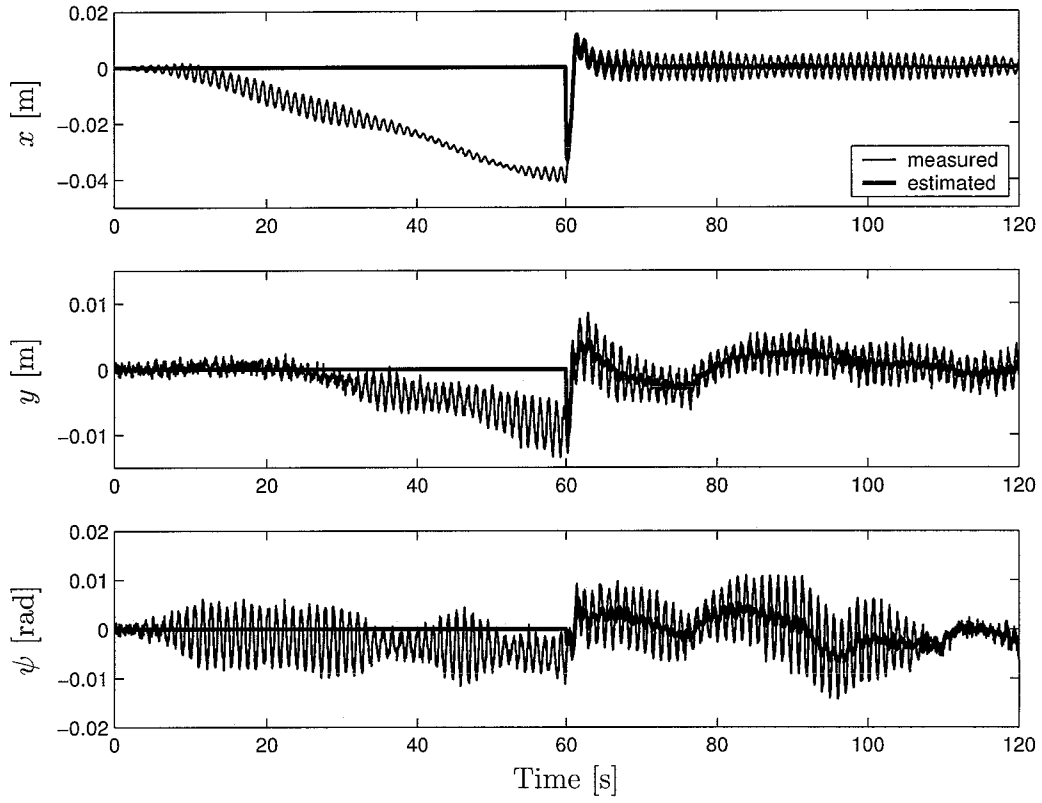

Figure 5.3: Simulation of the measured (thin line) and estimated (thick line) position using the total dynamic positioning system, switched on after 60 seconds.

Finally, as stated in section 4.5, the robustness for the added mass and damping parameters is to be investigated. This is necessary because these parameters are highly influenced by the presence of walls in the vicinity of the floating body and the water depth. From this analysis, it follows that the dynamic positioning system is robust for changes in these parameters. Even in cases with quite unrealistic parameter values, similar results to the ones in figure 5.3 are obtained.

5.3 Experimental Results

Next, the dynamic positioning system is tested on the experimental setup. Firstly, the observer is tested without the controller, for the wave frequency of $f = 0.94$ Hz. The results using only the observer are depicted in figure 5.4.

By comparing figure 5.4 with figure 5.2, it can be seen that, in the experiment, similar results are obtained as in the simulation. Namely, it is clear that the filtering of the first-order wave disturbances is not complete as some oscillatory motion remains in the filtered signal. However, because of the SPR-requirement of the observer, better filtering is not

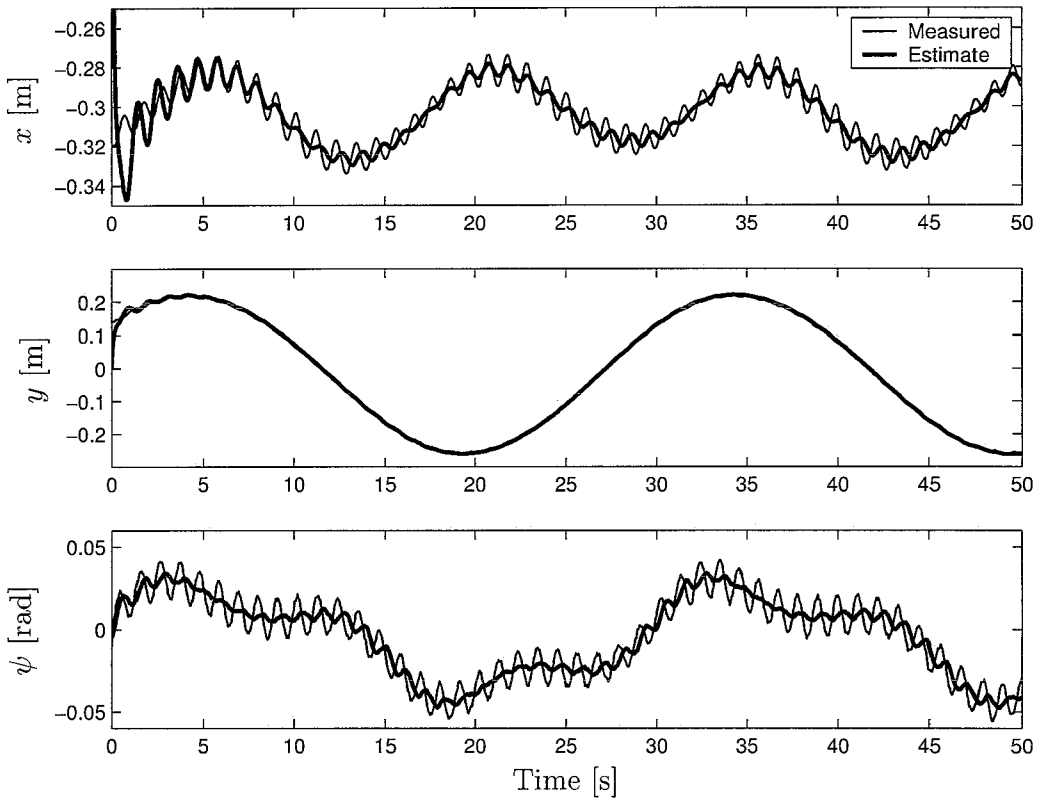

Figure 5.4: Experiment with the observer only. Measured (thin line) and estimated (thick line) position.

possible. A difference between the simulations and the experiments, however, is that the floating body undergoes large low-frequent periodic motions in the experiment, which are not modelled in the simulations (as stated in section 4.4). Although some first-order wave disturbances remain in the filtered signal, these low-frequent motions are estimated properly.

Finally, the complete dynamic positioning system is tested on the experimental setup. During testing, it is found that, due to hardware problems, it is impossible to use the dynamic positioning system for controlling *both* the sway- and yaw-directions at the same time. These hardware problems are probably caused by the coupling between the thrusters used for sway- and yaw-direction (both use thrusters 1–4), the threshold values in the thruster curves and the cable actuated position sensors influencing the yaw direction in particular. Moreover, the thruster motors run warm during operation, which can affect both the parameters f_{0i} and f_{1i} of the thruster curves. Naturally, not each thruster will be influenced in the same way. Furthermore, as discussed in section 4.3, the behaviour of the thrusters as a function of the input value is different for increasing and decreasing input values.

Therefore, only results for the dynamic positioning system are given with the controller active in surge and sway direction (tests using the controller in yaw-direction separately, show that it functions properly). In fact, this yields a 3 DOF system with actuators capable of influencing only 2 out of 3 DOFs. If all 3 degrees of freedom have to be controlled, the problem is that of an underactuated system, for which the observer and controller, proposed in chapter 3, are no longer valid. Linearising this system, similar to the approach in section 3.3.1, yields a system that is not controllable anymore. Therefore, different approaches should be used for controlling underactuated systems, but due to limited time, this has not been done.

However, without considering the yaw degree of freedom to be controlled, the system is controllable and not underactuated. This approach is followed here. Hence, only the stability analysis in chapter 3 changes, but this is omitted here.

During the experiment, the observer and controller are switched on after 60 seconds. The measured and estimated positions are depicted in figure 5.5. For completeness, the measurements and estimates in yaw-direction are also given.

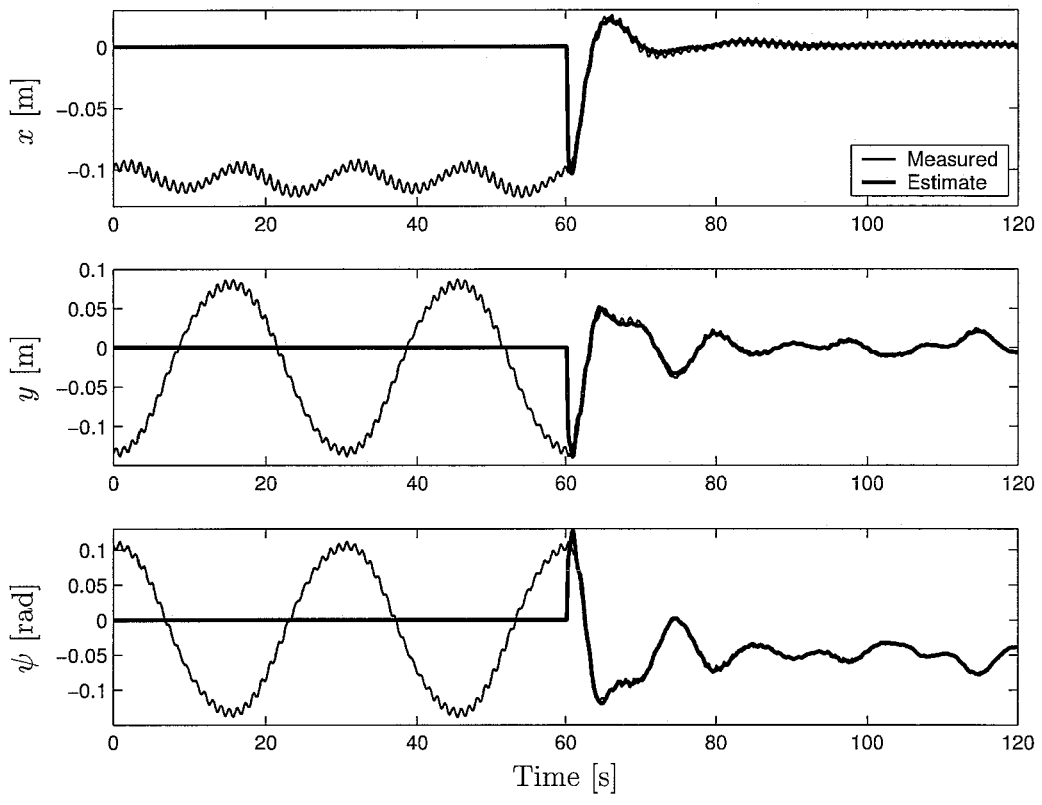

Figure 5.5: Experiment with the total dynamic positioning system in surge and sway direction only. Measured (thin line) and estimated (thick line) position are depicted.

As can be seen from figure 5.5, the DP system succeeds in stabilising the two DOFs considered around the origin. Additionally, it can be seen that both the measured and estimated heading angle are biased. This can be attributed to the thruster behaviour and the position measurement system, as described above.

Moreover, figure 5.6 shows the position of the centre of gravity of the floating body in the x-y-plane for this experiment. Here, it can be seen that the final accuracy obtained is about $\pm$ 0.003 m in x-direction and $\pm$ 0.02 m in y-direction, which is quite a satisfactory result for only two out of three degrees of freedom controlled, especially when the resolutions in table 4.2 are taken into account.

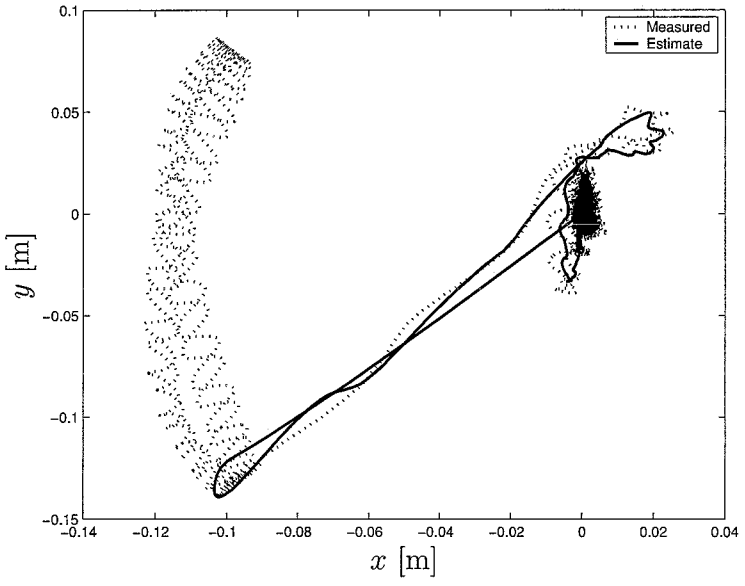

Figure 5.6: Measured (dotted) and estimated (solid) position in the x-y-plane during the experiment.

Finally, figure 5.7 shows a zoom plot of the X- and Y-components of the control $\boldsymbol{\tau}$. The threshold values in the thruster curves can be observed in this figure because only a certain minimum force can be generated. After some large thruster inputs in the beginning, it can be seen that, during the rest of the experiment, the thrusters have sufficient force for keeping the floating body on its place.

The tuning procedure for the observer and controller, is explained more in detail in appendix C, for easy use of the DP system with the experimental setup. Additionally, a description of the MATLAB- and LabVIEW-files, used to obtain these results, is given.

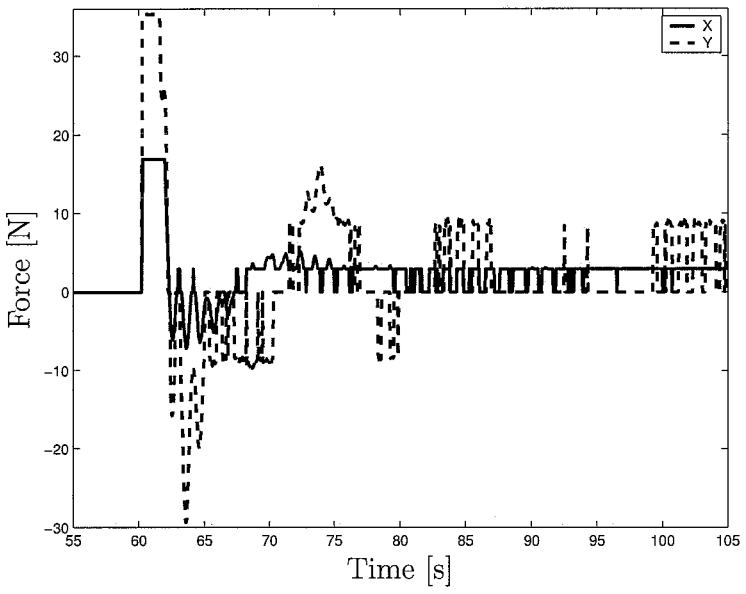

Figure 5.7: Zoom plot of the control τ in X- and Y-direction.

Chapter 6

Conclusions and Recommendations

In order to design a dynamic positioning system for a floating body in three degrees of freedom, firstly, a model has been derived to describe both the rigid-body dynamics and the environmental disturbances acting on the body. For the latter, a modelling method is chosen, that is suitable for control systems design.

The dynamic positioning system only has to compensate for the low-frequent second-order wave drift in the environmental disturbances and not for the first-order oscillatory motion caused by the waves. For this purpose, the dynamic positioning system consists of both an observer and a controller, designed using Lyapunov analysis. The non-linear observer can be designed to have the desired wave filtering properties, but has limited tuning freedom due to a strictly positive real requirement in its transfer function. This requirement is needed for concluding asymptotic stability. On the other hand, this results in a relatively straightforward tuning procedure for the observer. Furthermore, the controller – a PID controller with the non-linear rotation matrix included – is proven to be stable in a global sense when the maximum allowable yaw-rate exceeds the maximum achievable yaw-rate of the floating body. The complete dynamic positioning system, consisting of both the observer and controller, is also proven to be asymptotically stable in a global sense.

In the simulation model, the threshold values in the thruster characteristics are included, as these form an important property of the experimental system. Simulations with the dynamic positioning system show that, due to this behaviour, no asymptotic positioning is achieved, but small fluctuations around the desired position remain.

Tests with the system on the experimental setup show that, due to the influence of the cable actuated position sensors and the threshold values in the thruster curves, only the surge and sway degree of freedom can be controlled at the same time (the yaw-direction can, however, be controlled separately). Nevertheless, the dynamic positioning system

succeeds in stabilising the remaining degrees of freedom of the floating body around the origin with relatively small error bounds ($\pm$ 0.003 m in x-direction and $\pm$ 0.02 m in y-direction). More important, the maximum allowable yaw-rate using this controller by far exceeds the maximum achievable yaw rate of the system ($r_{max} = 28.7$ rad/s). Hence, an appropriate dynamic positioning system for two degrees of freedom is designed.

To improve the design of the dynamic positioning system and to overcome the difficulties in the experimental setup, the following recommendations can be made.

First, a solution to the threshold values in the motor characteristics should be found. This can either be done by choosing different motors, more capable of operating at low rotational velocities, or by altering the steering units for the motors, which control the rotational velocity, such that low rotational velocities can be generated more accurately.

Secondly, a contact-less position measurement system would overcome the difficulty that the cable actuated position sensors influence the degrees of freedom in an undesired way. Optical or hydroacoustic techniques could be used for this. Alternatively, linear and angular acceleration measurements with drift compensation could provide a solution.

Furthermore, to overcome the effect of the narrow notch in the observer transfer function, the observer could be made adaptive to the wave frequency. Consequently, due to the relatively straightforward tuning procedure, the observer gains could, in that case, be tuned automatically.

Moreover, it would be better to use a smaller floating body in the experimental setup. Namely, the present floating body has rather large inertia properties and is relatively large in comparison to the wave tank width. As a result, it causes a lot of disturbance in the wave field, thus influencing the hydrodynamic properties in an undesired way.

Finally, it would be worthwhile investigating the performance of more advanced controllers on the dynamic positioning problem, as only a simple PID-like controller has been used up till now.

Appendix A

Modelling of Marine Vehicles

A.1 Notation and Kinematics

The rigid-body motion of marine vehicles can be described by means of 6 degrees of freedom (DOF), since 6 independent coordinates are necessary to uniquely determine the position and the orientation of the vehicle. Three coordinates correspond to the translational motion along the x-, y- and z-axes, whereas the other three correspond to the orientation and rotational motion. For marine vehicles, these degrees of freedom are conveniently called *surge, sway* and *heave* for translational motions and *roll, pitch* and *yaw* for rotational motions. Moreover, for each degree of freedom, forces and moments are acting on the vehicle. These components, together with their time derivatives, are explained in table A.1.

Table A.1: Notation used for marine vehicles.

DOF		linear and angular velocity	position and Euler angles	forces and moments
1	motion in x-direction (surge)	u	x	X
2	motion in y-direction (sway)	v	y	Y
3	motion in z-direction (heave)	w	z	Z
4	rotation about the x-axis (roll)	p	ϕ	K
5	rotation about the y-axis (pitch)	q	θ	M
6	rotation about the z-axis (yaw)	r	ψ	N

In the analysis of marine vehicles, two coordinate frames are defined. (see figure A.1).

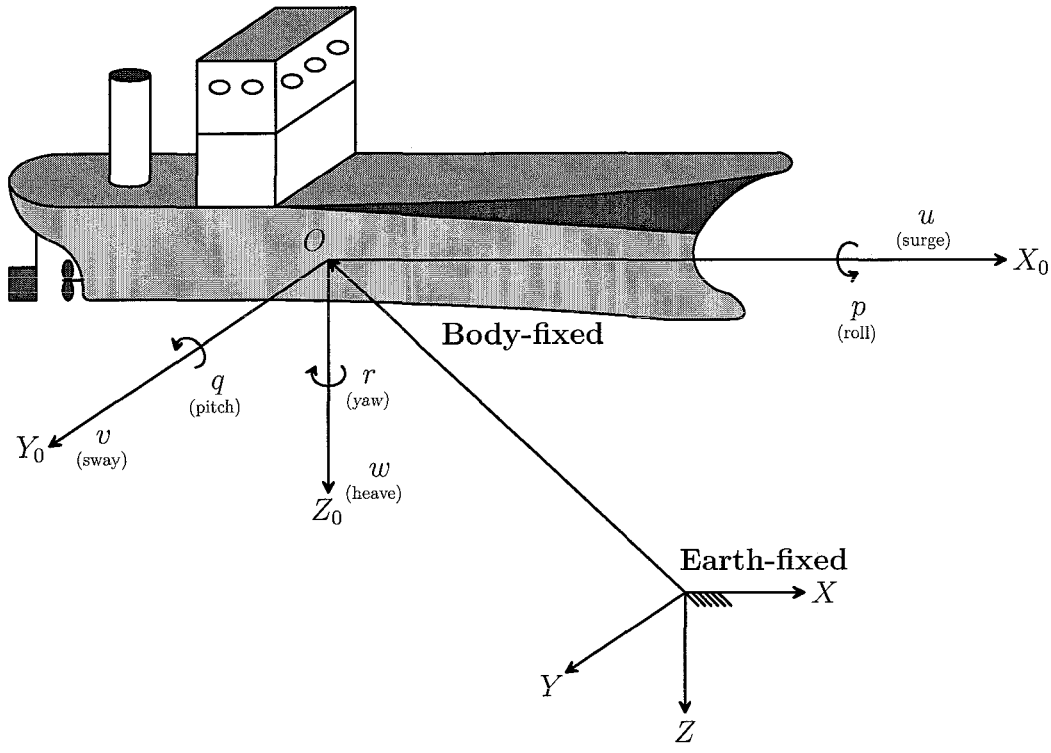

Figure A.1: Body-fixed and Earth-fixed reference frames.

The moving reference system $X_0Y_0Z_0$ is the so-called body-fixed reference frame. Commonly, the origin O of this system is chosen to coincide with the center of gravity (COG) of the vessel. The axes of the body-fixed frame are chosen along the principal axes of inertia of the vessel and are defined as:

- X_0 – longitudinal axis, directed from aft to fore,
- Y_0 – transverse axis, directed to starboard,
- Z_0 – normal axis, directed from top to bottom.

The motion of the body-fixed frame is described relative to an inertial reference frame or Earth-fixed frame. Hereby, it is assumed that the accelerations of a point on the surface of the Earth can be neglected, since the motion of the Earth hardly affects low speed marine vehicles. As a result, the Earth-fixed frame XYZ is an inertial frame.

In order to describe the position and the orientation of the marine vehicle, the following

vectors are defined:

$$\begin{aligned}
\boldsymbol{\eta} &= [\boldsymbol{\eta}_1^T, \boldsymbol{\eta}_2^T]^T; & \boldsymbol{\eta}_1 &= [x, y, z]^T; & \boldsymbol{\eta}_2 &= [\phi, \theta, \psi]^T, \\
\boldsymbol{\nu} &= [\boldsymbol{\nu}_1^T, \boldsymbol{\nu}_2^T]^T; & \boldsymbol{\nu}_1 &= [u, v, w]^T; & \boldsymbol{\nu}_2 &= [p, q, r]^T, \\
\boldsymbol{\tau} &= [\boldsymbol{\tau}_1^T, \boldsymbol{\tau}_2^T]^T; & \boldsymbol{\tau}_1 &= [X, Y, Z]^T; & \boldsymbol{\tau}_2 &= [K, M, N]^T.
\end{aligned}$$

Here, $\boldsymbol{\eta}$ denotes the position and orientation vector with coordinates in the earth-fixed reference frame and $\boldsymbol{\nu}$ denotes the linear and angular velocity vector with coordinates in the body-fixed frame. Finally, $\boldsymbol{\tau}$ describes the forces and moments acting on the vehicle in the body-fixed frame.

A.1.1 Velocity Transformations

The vehicle's path relative to the inertial space can be described by a velocity transformation:

$$\dot{\boldsymbol{\eta}}_1 = \boldsymbol{J}_1(\boldsymbol{\eta}_2)\boldsymbol{\nu}_1, \tag{A.1}$$

where $\boldsymbol{J}_1(\boldsymbol{\eta}_2)$ denotes a rotation matrix which depends on the Euler angles ϕ, θ and ψ. For the relation between the angular velocity vector $\boldsymbol{\nu}_2$ and the Euler rate vector $\dot{\boldsymbol{\eta}}_2 = [\dot{\phi}, \dot{\theta}, \dot{\psi}]$ a similar relation holds, namely:

$$\dot{\boldsymbol{\eta}}_2 = \boldsymbol{J}_2(\boldsymbol{\eta}_2)\boldsymbol{\nu}_2. \tag{A.2}$$

It should be noted that the angular velocity vector $\boldsymbol{\nu}_2$ cannot be integrated directly, as this has no physical meaning.

The velocity transformations are commonly described by a sequence of three rotations. The resulting expressions for the transformation matrices in (A.1) and (A.2) are given here, whereas the interested reader is referred to Fossen (1994) for the detailed computations.

$$\boldsymbol{J}_1(\boldsymbol{\eta}_2) = \begin{bmatrix} \mathrm{c}\psi\mathrm{c}\theta & -\mathrm{s}\psi\mathrm{c}\phi + \mathrm{c}\psi\mathrm{s}\theta\mathrm{s}\phi & \mathrm{s}\psi\mathrm{s}\phi + \mathrm{c}\psi\mathrm{c}\phi\mathrm{s}\theta \\ \mathrm{s}\psi\mathrm{c}\theta & \mathrm{c}\psi\mathrm{c}\phi + \mathrm{s}\phi\mathrm{s}\theta\mathrm{s}\psi & -\mathrm{c}\psi\mathrm{s}\phi + \mathrm{s}\theta\mathrm{s}\psi\mathrm{c}\phi \\ -\mathrm{s}\theta & \mathrm{c}\theta\mathrm{s}\phi & \mathrm{c}\theta\mathrm{c}\phi \end{bmatrix}, \boldsymbol{J}_2(\boldsymbol{\eta}_2) = \begin{bmatrix} 1 & \mathrm{s}\phi\mathrm{t}\theta & \mathrm{c}\phi\mathrm{t}\theta \\ 0 & \mathrm{c}\phi & -\mathrm{s}\phi \\ 0 & -\mathrm{s}\phi/\mathrm{c}\theta & \mathrm{c}\phi/\mathrm{c}\theta \end{bmatrix}, \tag{A.3}$$

where c·, s· and t· denote $\cos(\cdot)$, $\sin(\cdot)$ and $\tan(\cdot)$, respectively. Note that $\boldsymbol{J}_2(\boldsymbol{\eta}_2)$ is undefined for a pitch angle of $\theta = \pm 90°$. For surface vessels however, this will be no problem. Combining (A.1) and (A.2), the kinematic equations can be written in the following vector form:

$$\begin{bmatrix} \dot{\boldsymbol{\eta}}_1 \\ \dot{\boldsymbol{\eta}}_2 \end{bmatrix} = \begin{bmatrix} \boldsymbol{J}_1(\boldsymbol{\eta}_2) & \mathbf{0}_{(3\times3)} \\ \mathbf{0}_{(3\times3)} & \boldsymbol{J}_2(\boldsymbol{\eta}_2) \end{bmatrix} \begin{bmatrix} \boldsymbol{\nu}_1 \\ \boldsymbol{\nu}_2 \end{bmatrix} \quad \Rightarrow \quad \dot{\boldsymbol{\eta}} = \boldsymbol{J}(\boldsymbol{\eta})\boldsymbol{\nu}. \tag{A.4}$$

A.2 Rigid-Body Dynamics

The 6 DOF equations of motion for a marine vehicle can be derived by the Newton-Euler formulation or by the Lagrangian formulation. It is worthwhile mentioning that in the latter formulation a special principle has to be applied. Namely, in order to formulate the equations of motion in terms of the body-fixed reference frame, the generalized velocities $\boldsymbol{\nu} = [u, v, w, p, q, r]^T$ are used as generalized coordinates. Direct integration of the generalised angular velocities has no physical meaning. Therefore, Lagrange's equations in terms of quasi-coordinates have to be used (see Meirovitch, 1990).

The general 6 DOF rigid-body equations of motion are derived in Fossen (1994) and are, written in vector form, the following:

$$\boldsymbol{M}_{RB}\dot{\boldsymbol{\nu}} + \boldsymbol{C}_{RB}(\boldsymbol{\nu})\boldsymbol{\nu} = \boldsymbol{\tau}_{RB}, \tag{A.5}$$

where $\boldsymbol{M}_{RB} = \boldsymbol{M}_{RB}^T > 0$ is the positive definite rigid-body inertia matrix, $\boldsymbol{C}_{RB}(\boldsymbol{\nu}) = -\boldsymbol{C}_{RB}^T(\boldsymbol{\nu})$ is the matrix with Coriolis and centripetal terms and $\boldsymbol{\tau}_{RB} = [X, Y, Z, K, M, N]^T$ is a generalized vector with external forces and moments. As a simplified version of the equations of motion for dynamic positioning of ships is given in section 2.1.2, there is no need for giving the complete expressions for the matrices in equation (A.5) here.

A.3 Hydrodynamic Forces and Moments

A lot of different methods for the calculation of sea loads on ships are available in literature. One of the most popular, is a linear potential method, where the pressure field of the wetted surface is determined from superposition of the radiation and diffraction problem (see Faltinsen, 1990). These two sub-problems will be discussed next.

Radiaton-Induced Forces

Radiation-induced forces are the forces acting on the body when the body is forced to oscillate with the wave excitation frequency and there are no incident waves. These forces can be written as the sum of three components:

1. Added mass due to the inertia of the surrounding fluid,
2. Radiation-induced potential damping due to the energy carried away by the generated surface waves,
3. Restoring forces and moments due to Archimedes (weight and buoyancy).

The contribution of these forces ($\boldsymbol{\tau}_R$) can be written in vector form as (Fossen, 1994):

$$\boldsymbol{\tau}_R = -\boldsymbol{M}_A\dot{\boldsymbol{\nu}} - \boldsymbol{C}_A(\boldsymbol{\nu})\boldsymbol{\nu} - \boldsymbol{D}_P(\boldsymbol{\nu})\boldsymbol{\nu} - \boldsymbol{g}(\boldsymbol{\eta}). \tag{A.6}$$

Here, the first two terms in the right-hand side correspond to added mass contributions, $\boldsymbol{D}_P(\boldsymbol{\nu})$ is the potential damping term and $\boldsymbol{g}(\boldsymbol{\eta})$ contains the restoring forces. Moreover, in addition to potential damping, other damping effects have to be included:

$$\boldsymbol{\tau}_D = -\boldsymbol{D}_S(\boldsymbol{\nu})\boldsymbol{\nu} - \boldsymbol{D}_W(\boldsymbol{\nu})\boldsymbol{\nu} - \boldsymbol{D}_V(\boldsymbol{\nu})\boldsymbol{\nu}, \tag{A.7}$$

where $\boldsymbol{D}_S(\boldsymbol{\nu})$, $\boldsymbol{D}_W(\boldsymbol{\nu})$ and $\boldsymbol{D}_V(\boldsymbol{\nu})$ denote damping effects due to skin friction, wave drift damping and vortex shedding, respectively. The total radiation-induced and damping forces $\boldsymbol{\tau}_H$ can, hence, be written as the sum of equation (A.6) and (A.7):

$$\boldsymbol{\tau}_H = -\boldsymbol{M}_A\dot{\boldsymbol{\nu}} - \boldsymbol{C}_A(\boldsymbol{\nu})\boldsymbol{\nu} - \boldsymbol{D}(\boldsymbol{\nu})\boldsymbol{\nu} - \boldsymbol{g}(\boldsymbol{\eta}), \tag{A.8}$$

where the total damping matrix $\boldsymbol{D}(\boldsymbol{\nu})$ is defined as:

$$\boldsymbol{D}(\boldsymbol{\nu}) = \boldsymbol{D}_P(\boldsymbol{\nu}) + \boldsymbol{D}_S(\boldsymbol{\nu}) + \boldsymbol{D}_W(\boldsymbol{\nu}) + \boldsymbol{D}_V(\boldsymbol{\nu}). \tag{A.9}$$

Froude-Kriloff and Diffraction Forces

These are forces on the body when the body is restrained from oscillating and there are incident regular waves. These forces will be discussed in the context of environmental disturbances acting on the marine vessel in section A.4, which is a common approach in control systems design.

Combining the forces and moments acting on the body, as described above, the vector $\boldsymbol{\tau}_{RB}$ with generalized forces and moments in (A.5) can be written as:

$$\boldsymbol{\tau}_{RB} = \boldsymbol{\tau}_H + \boldsymbol{\tau}_E + \boldsymbol{\tau}. \tag{A.10}$$

Here, $\boldsymbol{\tau}_H$ is given in (A.8), $\boldsymbol{\tau}_E$ is a vector with environmental forces and moments and $\boldsymbol{\tau}$ is a vector with thruster forces. Inserting (A.8) in (A.10) and combining with (A.5) yields the following vectorial representation of the equations of motion:

$$\boldsymbol{M}\dot{\boldsymbol{\nu}} + \boldsymbol{C}(\boldsymbol{\nu})\boldsymbol{\nu} + \boldsymbol{D}(\boldsymbol{\nu}) + \boldsymbol{g}(\boldsymbol{\eta}) = \boldsymbol{\tau}_E + \boldsymbol{\tau}, \tag{A.11}$$

where $\boldsymbol{M} = \boldsymbol{M}_{RB} + \boldsymbol{M}_A$ and $\boldsymbol{C}(\boldsymbol{\nu}) = \boldsymbol{C}_{RB}(\boldsymbol{\nu}) + \boldsymbol{C}_A(\boldsymbol{\nu})$.

In the next three sections, the hydrodynamic terms in equation (A.11) will be discussed in detail.

A.3.1 Added Mass and Inertia

Often, added mass is misunderstood to be a finite amount of water connected to the submerged vehicle such that the vehicle and the fluid represent a new system with a mass larger than the original system. This is not true since the vehicle oscillations force the whole fluid to oscillate with a certain amplitude (which decays with increasing distance to the vehicle). Added (virtual) mass should, however, be understood as pressure-induced forces and moments acting on a body, which are proportional to the body's acceleration.

The added mass of a certain vehicle is frequency dependent and highly influenced by for example water depth and presence of reflecting surfaces in the vicinity of the vessel. Often, numerical packages are used to approximate the added mass coefficients. For positioned ships, it is a good approximation to assume the added mass matrix to be frequency *independent.* Moreover, the added mass coefficients are evaluated for zero frequency, as this asymptotic value is of interest for dynamic positioning. Hence, the added mass matrix is positive definite and symmetric: $\boldsymbol{M}_A = \boldsymbol{M}_A^T > 0$. Equivalently, the hydrodynamic matrix with Coriolis and centripetal terms is skew-symmetrical and also frequency independent: $\boldsymbol{C}_A(\boldsymbol{\nu}) = -\boldsymbol{C}_A^T(\boldsymbol{\nu})$.

A.3.2 Hydrodynamic Damping

As mentioned before, the hydrodynamic damping of an ocean vehicle is mainly caused by a combination of four damping components (see equation (A.9)), which will shortly be explained next.

Potential damping $\boldsymbol{D}_P(\boldsymbol{\nu})$ is radiation-induced damping due to the fact that an oscillation body generates waves that carry away energy. Similar to added mass, potential damping is frequency dependent. For low frequencies, however, potential damping does not occur as virtually no waves are generated in this case.

Skin friction damping $\boldsymbol{D}_S(\boldsymbol{\nu})$ can be split in two parts: linear skin friction is caused by laminar boundary layers and quadratic skin friction is caused by turbulent boundary layers. The linear part is most important when designing a control system for positioning of ships.

Wave drift damping $\boldsymbol{D}_W(\boldsymbol{\nu})$ can be seen as an added resistance for surface vessels moving through the waves. This damping is proportional to the square of the wave height.

Damping due to vortex shedding $\boldsymbol{D}_V(\boldsymbol{\nu})$ is damping in a viscous fluid which can be interpreted as a drag force acting on the vehicle.

It is difficult to obtain analytical expressions for all of these damping types. However, it can be stated that the hydrodynamic damping matrix (see equation (A.9)) is strictly positive ($\boldsymbol{D}(\boldsymbol{\nu}) > 0$), since damping forces are known to be dissipative.

A.3.3 Restoring Forces and Moments

In addition to the added mass and damping forces, a vessel will also be affected by restoring forces caused by the weight and buoyancy. These restoring forces are equivalent to the restoring forces in a mass-spring-damper system. These static considerations are referred to as *metacentric stability*, meaning that a metacentric stable vehicle will resist inclinations away from its static equilibrium point in the horizontal plane. The restoring forces and moments only influence the heave, pitch and roll movement of a marine vessel. Hence, for positioning of surface ships, these forces do not have to be taken into account as long as the ship is metacentric stable, which is assumed to be the case.

A.4 Environmental Disturbances

This section describes the environmental disturbances acting on a marine vessel and methods to model them. More specifically, three types of environmental disturbances can be considered:

- waves (wind generated),
- wind,
- ocean current.

In general, these disturbances are both multiplicative and additive to the dynamic equations of motion (A.11). However, it is assumed here, that the principle of superposition can be applied, which means that only additive disturbances are considered.

Furthermore, only waves can be generated in the experimental setup, as discussed in chapter 4. Therefore, the description of the other two disturbances is omitted. The interested reader is referred to Fossen (1994).

As mentioned in section A.3, the forces generated by waves are called Froude-Kriloff and diffraction forces. Generally, these forces can be considered as pressure forces and are computed by integrating these pressure forces over the wetted body surface. This pressure is both induced by the undisturbed waves and created by the vehicle when the waves are reflected from the vessel surface.

The method considered here, consists of splitting the environmental disturbances in first-order wave disturbances (relatively high-frequent motions) and second-order wave drift. This will be discussed in the next two sections.

A.4.1 First-Order Wave Disturbances

The motion of waves is normally observed to have only one or a few dominant frequencies. The first-order wave disturbances consist of the wave-induced oscillatory motion that a vessel undergoes. In control system engineering, it is common to model this oscillatory motion by a linear approximation to the wave spectrum in the form of a transfer function (see for example Fossen, 1994). For simplicity, it is assumed in these models that the wave spectrum only has one dominant frequency. This wave model can be written in the frequency domain as:

$$y(s) = h(s)w(s), \tag{A.12}$$

where $y(s)$ is the wave elevation, $h(s)$ is the wave transfer function approximation and $w(s)$ is a zero mean Gaussian white noise process with unit intensity. Often, a damped oscillator is used for modelling the transfer function $h(s)$ for each DOF:

$$h(s) = \frac{k_{wi}s}{s^2 + 2\xi_i\omega_{0i}s + \omega_{0i}^2}, \tag{A.13}$$

where k_{wi} denotes the wave intensity for DOF i, ω_{0i} denotes the dominant wave frequency and ξ_i is the relative damping coefficient in direction i. Typically, ξ_i is chosen < 1.

To obtain a better representation, a fourth-order wave transfer function approximation for each DOF can be used (Lindegaard, 2003), which is given by:

$$h(s) = \frac{k_{wi}s}{(s^2 + 2\xi_i\omega_{0i}s + \omega_{0i}^2)^2}. \tag{A.14}$$

A realisation of this transfer function in state-space for a single DOF with $\boldsymbol{x}_w \in \mathbb{R}^4$ can be written as:

$$\dot{\boldsymbol{x}}_w = \boldsymbol{A}_w\boldsymbol{x}_w + \boldsymbol{E}_w w_w, \tag{A.15}$$

$$y_w = \boldsymbol{C}_w\boldsymbol{x}_w, \tag{A.16}$$

$$\boldsymbol{A}_w = \begin{bmatrix} 0 & 1 & 0 & 0 \\ -\Omega_i & -\Lambda_i & 0 & 1 \\ 0 & 0 & 0 & 1 \\ 0 & 0 & -\Omega_i & -\Lambda_i \end{bmatrix}, \quad \boldsymbol{E}_w = \begin{bmatrix} 0 \\ 0 \\ 0 \\ k_{wi} \end{bmatrix}, \quad \boldsymbol{C}_w = \begin{bmatrix} 1 & 0 & 0 & 0 \end{bmatrix}. \tag{A.17}$$

Here, scalars $\Omega_i = \omega_{0i}^2$ and $\Lambda_i = 2\xi_i\omega_{0i}$ are introduced to simplify the notation. Figure A.2 shows a typical representation of this wave transfer function approximation.

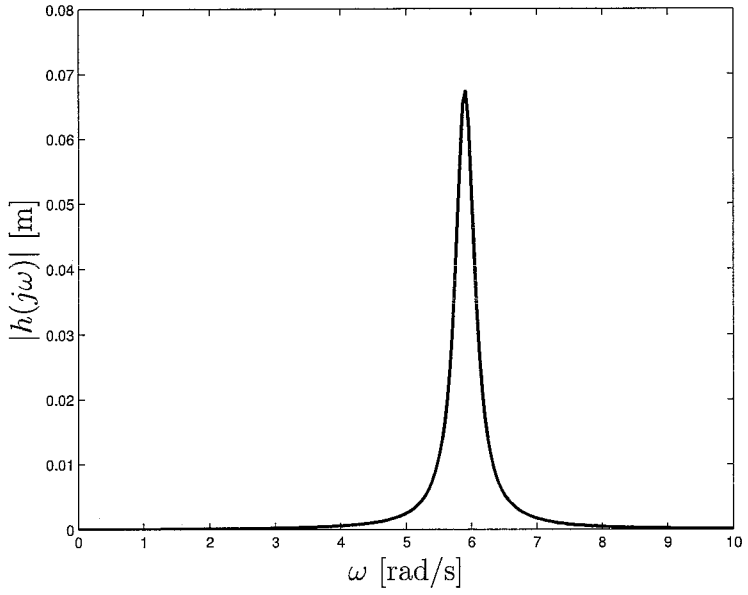

Figure A.2: Example of a wave transfer function approximation. The parameters are chosen as $\omega_{0i} = 1.88\pi$ rad/s, $\xi_i = 0.03$ and $k_{wi} = 0.05$.

For ships moving with a forward speed U, the dominant wave frequency would have to be modified. For positioned ships, however, this so-called frequency of encounter equals the dominant wave frequency.

A.4.2 Second-Order Wave Drift

Waves acting on a vessel induce forces on it. These forces are, in control applications, often modelled as bias forces acting on the vessel. A suitable model for describing these bias forces is a first-order Markow process:

$$\dot{\boldsymbol{b}} = -\boldsymbol{T}_b^{-1}\boldsymbol{b} + \boldsymbol{E}_b\boldsymbol{w}_b. \tag{A.18}$$

Here, $\boldsymbol{b}$ is a vector with bias forces and moments, $\boldsymbol{T}_b$ is a diagonal matrix with bias time constants T_{bi} $(i = 1, \ldots, 6)$ (typically chosen large), $\boldsymbol{w}_b$ is a vector of zero mean Gaussian white noise processes and $\boldsymbol{E}_b$ is a diagonal matrix scaling the amplitude of $\boldsymbol{w}_b$. The bias model accounts for slowly varying forces and moments due to second-order wave loads. In addition, the bias model will account for slowly-varying unmodelled dynamics and actuator thrust losses (Strand, 1999).

Appendix B

Position Measurement

B.1 General Idea

In section 4.2, it is elucidated that the position of the floating body is determined by means of 6 cable actuated position sensors. This section describes the derivation of the equations that are necessary obtain the position vectors of the front and the back of the floating body. In figure B.1, a schematic representation of the floating body can be seen, where the sensors are numbered as in the experimental setup.

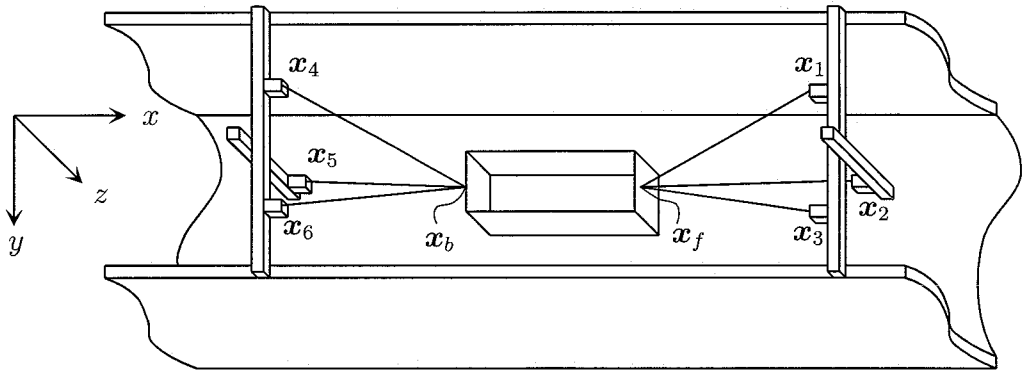

Figure B.1: Schematic representation of the floating body and the cable actuated position sensors.

The sensor position vectors $\boldsymbol{x}_i = [x_i, y_i, z_i]^T$ $(i = 1, \ldots, 6)$, relative to a wave tank fixed origin, are measured and given in table 4.1. The sensor coordinates satisfy the following properties:

$$x_1 = x_3, \qquad z_1 = z_3, \tag{B.1}$$

$$x_4 = x_6, \qquad z_4 = z_6. \tag{B.2}$$

Note, that these relations can always be satisfied by defining two separate coordinate systems for the front and back side. Here, however, the sensors are *positioned* such that, in addition to (B.1) and (B.2), $z_1 = z_3 = z_4 = z_6$ holds (see table 4.1) and the x-axes are parallel. Therefore, only one coordinate system is necessary for describing the sensor positions.

From the six wire lengths l_i $(i = 1, \ldots, 6)$, the positions $\boldsymbol{x}_f = [x_f, y_f, z_f]^T$ and $\boldsymbol{x}_b = [x_b, y_b, z_b]^T$ have to be determined. Consider the front of the floating body in figure B.1, where sensors 1,2 and 3, with wire length l_1, l_2 and l_3, respectively, uniquely determine $\boldsymbol{x}_f$. Namely, this point has to lie on the intersection of three balls, located in position $\boldsymbol{x}_i$ with radius l_i $(i = 1, 2, 3)$. This gives two solutions, one on each side of the position sensors. Due to geometry considerations, only one of these solutions is valid and, hence, the position vector is known. This will be explained in the next section.

B.2 Calculation of the Position Vectors

For the front side of the floating body, the equations for the three balls are given as:

$$l_1^2 = (\boldsymbol{x}_1 - \boldsymbol{x}_f)^T(\boldsymbol{x}_1 - \boldsymbol{x}_f), \tag{B.3}$$

$$l_2^2 = (\boldsymbol{x}_2 - \boldsymbol{x}_f)^T(\boldsymbol{x}_2 - \boldsymbol{x}_f), \tag{B.4}$$

$$l_3^2 = (\boldsymbol{x}_3 - \boldsymbol{x}_f)^T(\boldsymbol{x}_3 - \boldsymbol{x}_f), \tag{B.5}$$

or, written in component-form:

$$l_1^2 = (x_1 - x_f)^2 + (y_1 - y_f)^2 + (z_1 - z_f)^2, \tag{B.6}$$

$$l_2^2 = (x_2 - x_f)^2 + (y_2 - y_f)^2 + (z_2 - z_f)^2, \tag{B.7}$$

$$l_3^2 = (x_3 - x_f)^2 + (y_3 - y_f)^2 + (z_3 - z_f)^2. \tag{B.8}$$

By subtracting (B.8) from (B.6) and applying (B.1), the following results:

$$(y_1 - y_f)^2 - (y_3 - y_f)^2 = l_1^2 - l_3^2. \tag{B.9}$$

This equation can be solved for the y-position of the point at the front of the body, yielding

$$y_f = \frac{l_1^2 - y_1^2 - l_3^2 + y_3^2}{2(y_3 - y_1)}. \tag{B.10}$$

Next, this value is used in equations (B.6) and (B.7) to obtain:

$$(x_1 - x_f)^2 + (z_1 - z_f)^2 = \underbrace{l_1^2 - (y_1 - y_f)^2}_{c_1}, \tag{B.11}$$

$$(x_2 - x_f)^2 + (z_2 - z_f)^2 = \underbrace{l_2^2 - (y_2 - y_f)^2}_{c_2}, \tag{B.12}$$

where the right-hand sides are conveniently written as c_1 and c_2, respectively. Next, subtracting (B.12) from (B.11) gives

$$(x_1 - x_f)^2 - (x_2 - x_f)^2 + (z_1 - z_f)^2 - (z_2 - z_f)^2 = c_1 - c_2, \tag{B.13}$$

which can be solved for z_f as a function of x_f:

$$z_f = \underbrace{\frac{c_1 - x_1^2 - z_1^2 - c_2 + x_2^2 + z_2^2}{2(z_2 - z_1)}}_{a_f} \underbrace{-\frac{x_2 - x_1}{z_2 - z_1}}_{b_f} x_f. \tag{B.14}$$

To save space, variables a_f and b_f are introduced (see equation (B.14)), such that

$$z_f = a_f + b_f x_f. \tag{B.15}$$

Now, (B.15) is inserted in (B.11) and, after some manipulation, the following quadratic equation in x_f is found:

$$(1 + b_f^2)x_f^2 + (2a_f b_f - 2z_1 b_f - 2x_1)x_f + x_1^2 - c_1 + (z_1 - a_f)^2 = 0. \tag{B.16}$$

By redefining the terms in (B.16) as

$$A_f = 1 + b_f^2, \tag{B.17}$$

$$B_f = 2a_f b_f - 2z_1 b_f - 2x_1, \tag{B.18}$$

$$C_f = x_1^2 - c_1 + (z_1 - a_f)^2, \tag{B.19}$$

the roots of this equation can be found from the ABC-formula:

$$x_f = \frac{-B_f \pm \sqrt{B_f^2 - 4A_f C_f}}{2A_f}. \tag{B.20}$$

By considering figure B.1 together with the sensor coordinates in table 4.1, it can be seen that only one solution is valid, namely

$$x_f = \frac{-B_f + \sqrt{B_f^2 - 4A_f C_f}}{2A_f}. \tag{B.21}$$

In this way, the position $\boldsymbol{x}_f = [x_f, y_f, z_f]^T$ can be determined from equations (B.21), (B.10) and (B.15). The position vector $\boldsymbol{x}_b$ can be determined in a similar way, with the only difference, that the other solution of the ABC-formula is used.

From the positions of the two points on the floating body, the coordinates x, y and ψ, relative to the origin O, can be derived by considering figure B.2.

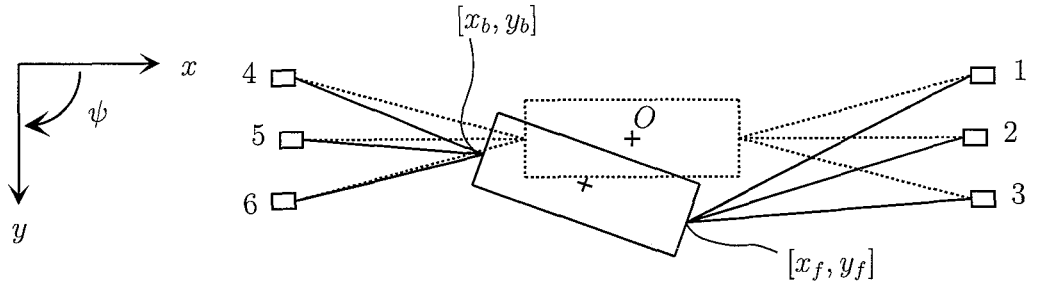

Figure B.2: Top-down view of the floating body.

From this figure, it can clearly be seen that the following relations hold:

$$x = -\frac{x_f + x_b}{2}, \tag{B.22}$$

$$y = \frac{y_f + y_b}{2}, \tag{B.23}$$

$$\psi = \arctan\left(\frac{y_f - y_b}{x_b - x_f}\right). \tag{B.24}$$

The minus sign is added in (B.22), because the sensor positions are measured with the x-direction opposite to the one depicted in figure B.2. For the heading angle, it holds that $-90° \leq \psi \leq 90°$, due to the limited range for the sensors. Therefore, the positions and the heading angle are uniquely determined.

Appendix C

Tuning Procedure

C.1 File Description

The file description consists of three parts. Firstly, m-files, for command-line use in MATLAB are given. Next, the SIMULINK model-files are described and, finally, the LabVIEW-files are given.

Matlab m-files.
In table C.1, a description of the m-files, needed for the use of the dynamic positioning system, is given. All of the files, except the first one, need the general input-file `sim_input.m`.

Table C.1: M-file Description.

`sim_input.m`	Initialisation file with the simulation parameters. This file contains three parts: (1) a part with the tuning parameters, (2) a part with the fixed parameters and (3) a part with the parameters for SIMULINK.
`calc_rmax.m`	File to calculate the maximum allowable yaw-rate for concluding stability of the controller (calculated using LMI-techniques for which the LMI-toolbox is needed in MATLAB).
`check_SPR.m`	File to check the Strictly Positive Realness of the observer, needed for concluding stability
`ship_robust.m`	File to examine the robustness properties of the closed loop system under a change of parameters. This robustness is expressed in terms of the location of the closed-loop poles and the maximum allowable yaw-rate (once again, the LMI-toolbox is required in MATLAB).

Table C.1: M-file Description.

`sim_ship.m`	File to simulate the behaviour of the floating body without observer or controller.
`sim_obs.m`	File to simulate the behaviour of the ship model together with the observer model.
`sim_contr.m`	File to simulate the behaviour of the ship mode with the controller only.
`sim_obs_contr.m`	File to simulate the behaviour of the complete DP system, that is, the ship model with the observer and controller included.
`wave_position.m`	File to compare the measurements from `position_main.vi` with simulations from `ship.mdl`, such that the wave and bias model can be tuned by means of the time responses and the spectrum.
`plot_obs_only.m`	File to plot the measurements from `obs_only.mdl`.
`plot_complete.m`	File to plot the results from the measurements from the complete Dynamic Positioning system.

Simulink model-files.

The model files are given in table C.2.

Table C.2: Model-file Description.

`ship.mdl`	Model-file that contains the ship model.
`ship_obs.mdl`	Model file that contains the ship model and the observer.
`ship_contr.mdl`	Model file that contains the ship model and the controller.
`ship_obs_contr.mdl`	Model file that contains the total dynamic positioning system.
`position.mdl`	Model file that contains the position measurement part for use with LabVIEW.
`obs_only.mdl`	Model file that contains the observer for use with LabVIEW.
`contr_only.mdl`	Model file that contains the controller without observer for use with LabVIEW
`complete.mdl`	Model file that contains the complete Dynamic Positioning system for use with LabVIEW.

LabVIEW Virtual intruments.
For LabVIEW, the following virtual Instruments (VI's) are available (table C.3), each located in a separate folder containing the necessary sub-VI's:

Table C.3: LabVIEW Virtual Instruments.

`position_main.vi`	VI that measures the position of the floating body (belongs to the SIMULINK model `position.mdl`).
`observer_main.vi`	VI that contains the position measurement and the observer (belongs to the SIMULINK model `obs_only.mdl`).
`controller_main.vi`	VI that contains the position measurement and the controller *without* observer (belongs to the SIMULINK model `contr_only.mdl`).
`complete_main.vi`	VI that contains the complete Dynamic Positioning system (belongs to the SIMULINK model `complete.mdl`).

Model use and compilation.
The models for use in LabVIEW in table C.2 are used as follows:

- `sim_input.m` is run
- The relevant SIMULINK model is opened in MATLAB by (for example): `open complete.mdl`
- LabVIEW is shut down in case it is still running
- The model is compiled by pressing [Ctrl]+[B]
- The generated `.DLL`-file is copied into the relevant LabVIEW folder
- The LabVIEW model is started
- After stopping the experiment, the relevant `.mat` data-file is to be copied into the folder where the MATLAB m-files, described in table C.1, are located.

C.2 General Tuning Procedure

In order to obtain a working dynamic positioning system, the following tuning procedure is advised, where it is assumed that the system parameters do not need to be modified. In general, it is advisable to run `sim_input.m` before every compilation, to make sure that the right parameters are available in the workspace of MATLAB.

- Appropriate simulation parameters are set in `sim_input.m`
- The position measurement device is switched on
- `sim_input.m` is executed and `position.mdl` is opened and compiled ([Ctrl]+[B])
- The rest position of the body is checked using `position_main.vi`
- A frequency and voltage is set for the wave flap in the signal generator and the wave generator is switched on
- `position_main.vi` is started and a measurement is performed for preferably 150 or 300 seconds. Note that incorrect spectra will be calculated from the position measurement if not all the cables for measuring the position are under tension! The file that is generated (`position.mat`) is copied into the appropriate MATLAB-folder.
- using `wave_position.m`, the parameters for the wave and bias model (frequency, damping and variances) are tuned in `sim_input.m`, such that the measurements are matched. This happens both by matching in the time domain (drift model) and in frequency domain (wave model and measurement noise).
- The observer is designed to be Strictly Positive Real by tuning the observer parameters in `sim_input.m` and plotting the transfer functions using `check_SPR.m` (in order to do this, the dimensionless damping coefficient in the observer (ξ_{ni}) has to be chosen approximately three times as large as the one in the wave model)
- The observer is tested in simulation by using `sim_obs.m`
- The observer is tested on the experimental setup using `observer_main.vi` (after `obs_only.mdl` is compiled), until it works satisfactorily. To check this, the generated `obs_only.mat` is copied into the MATLAB-folder and `plot_obs_only.m` is executed.
- A controller is designed by modifying the tuning parameters in `sim_input.m` Increasing the gain gives better results, but do not increase it too much because of the limited filtering properties of the observer
- The controller is tested in simulation by running `sim_obs_contr.m`
- The degrees of freedom to be controlled are selected in `sim_input.m`
- `complete.mdl` is compiled and `complete_main.vi` is started in LabVIEW. The DP system can be switched on manually
- `complete.mat` is copied into the MATLAB-folder and `plot_complete.m` is executed.

Bibliography

Faltinsen, O. M. (1990). *Sea Loads on Ships and Offshore Structures.* Cambridge University Press.

Fossen, T. I. (1994). *Guidance and Control of Ocean Vehicles.* John Wiley & Sons.

Fossen, T. I. and Strand, J. P. (1999). Passive Nonlinear Observer Design for Ships using Lyapunov Methods: Full-Scale Experiments with a Supply Vessel. *Automatica*, 35(1):3–16.

Fung, P. T.-K. and Grimble, M. J. (1983). Dynamic Ship Positioning Using a Self-Tuning Kalman-Filter. *IEEE Transactions on Automatic Control*, AC-28(3):339–350.

Gahinet, P., Nemirovski, A., Laub, A. J., and Chilali, M. (1995). *LMI Control Toolbox.* The Mathworks inc.

Khalil, H. K. (1996). *Nonlinear Systems.* Prentice Hall Inc.

Lindegaard, K.-P. W. (2003). *Acceleration Feedback in Dynamic Positioning.* PhD thesis, Department of Engineering Cybernetics, Norwegian Institute of Technology, Trondheim.

Lindegaard, K.-P. W. and Fossen, T. I. (2003). Fuel Efficient Rudder and Propellor Control Allocation for Marine Craft: Experiments with a Model Ship. *IEEE Transactions on Control Systems Technology*, To appear.

Meirovitch, L. (1990). *Dynamics and Control of Structures.* Wiley Interscience, NY.

Panteley, E. and Loria, A. (1998). On Global Uniform Asymptotic Stability of Nonlinear Time-Varying Systems in Cascade. *Systems & Control Letters*, 33(2):131–138.

Strand, J. P. (1999). *Nonlinear Position Control Systems Design for Marine Vessels.* PhD thesis, Department of Engineering Cybernetics, Norwegian Institute of Technology, Trondheim.

Acknowledgements

I am very thankful to a number of people for their help with and contributions to my project.

Firstly, I would like to thank professor Kreuzer and professor Nijmeijer for their effort on establishing the student exchange program between Technical University of Hamburg-Harburg and the Eindhoven University of Technology.

Furthermore, I am very grateful to my coach Marc-André Pick, with whom I spent a lot of time in getting the experimental setup to work properly. Also, his efforts in constructing the floating body should not remain unnoticed. I also thank him for the interesting discussions on my project during these 3.5 months. I gained a lot of theoretical and practical insight.

Also, I thank Mr. Schlegel for the various discussions we had, both related to my project and to a variety of other topics.

I wish to express my gratitude to Mrs. Andrlik, who did a very good job in finding a room for me.

Next, I would like to thank the people at the lab, Thilien, Wolfgang, Riza and Norbert, for their practical assistance with the construction of the floating body and the experimental setup. You have been a great help.

I am grateful to Marc-André, Henning and Andreas for the company outside the university. We had a very good time together.

Finally I would like to thank all colleagues at the Mechanics and Ocean Engineering department for the numerous coffee breaks, discussions and meals we had together.

Rob Mestrom,

January 2004.